Variations of Mg isotope geochemistry in soils over a Hawaiian 4 Myr chronosequence

Jong-Sik Ryu, Nathalie Vigier, Louis Derry, Oliver Chadwick

Variations of Mg isotope geochemistry in soils over a Hawaiian 4 Myr chronosequence

Jong-Sik Ryu[1,*], Nathalie Vigier[2], Louis Derry[3], Oliver A. Chadwick[4]

[1] Department of Earth and Environmental Sciences, Pukyong National University, Busan 48513, South Korea
[2] LOV, CNRS, UPMC, UMR 7093, 181 chemin du Lazaret, 06230 Villefranche-sur-Mer, France
[3] Department of Earth and Atmospheric Science, Cornell University, NY 14853, USA
[4] Department of Geography, University of California, Santa Barbara, CA 93106, USA

Number of tables: 5 including Supplementary Information
Number of figures: 7 including Supplementary Information
Number of words in the abstract: 281

Original version resubmitted to *Geochimica et Cosmochimica Acta* on August 16, 2019
3rd revised version submitted to *Geochimica et Cosmochimica Acta* on September 18, 2020

[*]Author to whom correspondence should be addressed: Phone (+82-51-6296624), FAX (+82-51-6296623), and e-mail (jongsikryu@gmail.com)

ABSTRACT

Magnesium (Mg) isotopes fractionate during rock/mineral weathering and leaching, secondary mineral neoformation, adsorption/desorption, and plant-related Mg recycling, but the mechanisms and extent of fractionation are not well understood. Here, we report the fate of Mg and its isotopes during weathering and soil development in the Hawaiian Islands by sampling soils of varying age (0.3, 20, 150, 1,400, and 4,100 ka) in undisturbed humid rainforests. Magnesium concentrations in bulk soils are variable with depth and age, ranging from 0.07 to 8.79 wt.%, and significant Mg depletions (up to 99%) relative to parent basalts are visible after 20 ka. Bulk soils display a large age-dependent range of δ^{26}Mg values ranging from −0.60 to +0.26‰. A sequential leaching scheme showed that labile Mg is depleted whereas residual Mg is enriched in isotopically heavy Mg. The two youngest soils (0.3 ka) display δ^{26}Mg value similar to basalt for both labile or residual Mg, indicating either that basalt weathering causes little Mg isotope fractionation or that δ^{26}Mg value is overwhelmed by the primary minerals during 0.3 ka. However, in the older soils (≥ 20 ka), the δ^{26}Mg values of both labile and residual Mg vary non-linearly as a function of time, with an increase in the difference between them. These variations are explained by both plant-related Mg recycling and progressive mineral transformations, evolving from short-range-order (SRO) minerals (allophane and ferrihydrite) to more crystalline products (goethite, gibbsite and kaolin minerals). Indeed, plant-related Mg recycling causes the enrichment of light Mg isotopes in the labile Mg, while crystalline secondary phases incorporate more and more heavy Mg isotopes with time. These results reconcile experimental and field studies and highlight a weathering control of Mg isotopes delivered to the oceans.

Keywords: Magnesium isotopes; Secondary minerals; Isotope fractionation; Basalt weathering; Soil; Hawaii

1. INTRODUCTION

The release of cations, especially calcium (Ca) and magnesium (Mg), from silicate rocks during chemical weathering is one of the most important processes controlling long-term climate change, seawater chemistry and nutrient cycling in soils (Berner et al., 1983; de Villiers and Nelson, 1999; Berner, 2004). Basalt weathering is important in terms of global carbon cycle because it accounts for about 35% of the global CO_2 sink associated with silicate weathering while basalt covers less than 5% of the overall continental area (Dessert et al., 2003). In parallel, basalt weathering exports considerable amount of major and trace elements, and nutrients to the ocean via river transport (Dessert et al., 2001, 2003).

In this context, non-traditional stable isotopes, such as lithium, calcium, and magnesium isotopes, can be used to trace silicate weathering and reconstructing paleo-climate (e.g., Tipper et al., 2006, 2008a; Vigier et al., 2009; Misra and Froelich, 2012; Pogge von Strandmann et al., 2008, 2012, 2013; Ryu et al., 2014). However additional work is needed to provide clear linkages between fractionation processes occurring in natural Earth surface systems and those deduced from experimental studies. Many studies indicate that significant Mg isotope fractionation occurs during rock/mineral dissolution, secondary mineral neoformation, adsorption/desorption, plant uptake/decomposition and recycling (e.g., Tipper et al., 2006, 2008a; Black et al, 2008; Pogge von Strandmann et al., 2008; Teng et al., 2010; Wimpenny et al., 2010, 2014; Ryu et al., 2011, 2016; Bolou-Bi et al., 2010, 2012; Huang et al., 2012; Lee et al., 2014; Liu et al., 2014; Opfergelt et al., 2014; Gao et al., 2018). However, reported directions of Mg isotope fractionation appear contradictory. For example, dissolution experiments show that light Mg isotopes are preferentially released during primary olivine dissolution (Wimpenny et al., 2010), even as other studies indicate little apparent Mg isotope fractionation between solution

92 and primary phases (Ryu et al., 2016). Also some experimental studies indicate small but
93 significant isotope fractionation during preferential incorporation of light Mg isotopes into
94 secondary minerals, such as chrysotile, brucite, saponite and stevensite (Wimpenny et al., 2010;
95 Li et al., 2014; Hindshaw et al., 2020). In contrast, other phases, such as brucite, kerolite and
96 lizardite have shown preferential incorporation of heavy Mg isotopes (Wimpenny et al., 2014;
97 Ryu et al., 2016). Likewise, field studies have reported both enrichment in light and heavy Mg
98 isotopes in soil minerals. Some studies suggest that secondary minerals have heavy Mg isotope
99 compositions due to either the preferential incorporation of heavy Mg isotopes into mineral
100 lattice, or the adsorption of heavy Mg isotopes onto mineral surface/interlayer (Tipper et al.,
101 2006; Teng et al., 2010; Huang et al., 2012; Opefergelt et al., 2012; Liu et al., 2014; Gao et al.,
102 2018), but the opposite was also shown (Pogge von Strandmann et al., 2008). An experimental
103 study by Hindshaw et al. (2020) suggests that the direction of Mg isotope fractionation depends
104 on the difference in the Mg–O bond length between a crystal lattice and solution. Although the
105 number of experimental studies has increased, few investigations have focused on natural
106 weathering profiles drawn from clear geological and ecological contexts. As a consequence, we
107 lack clarity on Mg isotope fractionation during key soil forming processes.
108 Here, we examine processes responsible for Mg isotope fractionation in basaltic soils
109 collected along a well-known humid-environment chronosequence in the Hawaiian Islands (e.g.
110 Vitousek et al. 1997; Vitousek, 2004; Chadwick et al., 1999, 2009; Chorover et al., 2004;
111 Wiegand et al., 2005; Ziegler et al., 2005; Pett-Ridge et al., 2007). This chronosequence allows
112 us to better understand the fate of Mg and its isotopes from the initial stages of basalt leaching to
113 the slow accumulation of metastable secondary minerals and their eventual reorganization into
114 relatively inert secondary crystalline phases (secondary mineral formation). We also assess the

role of atmospheric deposition and vegetation assimilation and release of Mg. This study provides new insights into understanding the behavior of Mg isotopes during basalt weathering and secondary mineral transformation as a function of age as well as the biogeochemical cycle of Mg closely related to the long-term CO_2 cycle.

2. MATERIALS AND METHODS

2.1. Study area

Detailed descriptions of the study area are given in previous studies (Crews et al., 1995; Vitousek et al., 1997; Vitousek, 2004; Ryu et al., 2014). In short, the Hawaiian chronosequence considered here varies in age from 0.3 ka to 4100 ka and has been referred to as the "Long-Substrate Age Gradient (LSAG)" (Vitousek et al., 1997). All six sites where the profiles have developed in lava mixed with tephra with subsrate ages of 0.3, 20, 150, 1400, and 4100 ka are near 1200 m elevation, receive 2500 mm annual rainfall, and have a mean annual temperature of 15°C. The soils and climate support rain forests composed of primarily of *Metrosideros polymorpha* and *Cibotium spp* (Vitousek, 2004). The two youngest sites (0.3 ka; Thurston (Th) and Ola'a (Ol)) are in Keanakakoi tephra derived from phreatomagmatic eruptions of tholeiitic composition at the summit of Kilauea (McPhie et al., 1990; Fiske et al., 2009), while the older sites (≥ 20ka) are composed of alkali basalt, such as hawaiite, mugearite, and their associated tephra (MacDonald et al., 1983; Wright and Heltz, 1986; Wolfe and Morris, 1996). All soils are located on primary shield volcano surfaces, where physical erosion and groundwater influences are minimal. Although the two youngest soils are Andisols dominated by primary basaltic material (glass, plagioclase, augite, olivine, magnetite, and ilmenite), primary volcanic minerals and volcanic glass are absent and are replaced by non-crystalline secondary minerals in soils 20

ka and older (Kurtz et al., 2001). The two intermediate-age soils, 20 ka and 150 ka, are highly weathered Andisols composed of chemically active metastable secondary minerals such as ferrihydrite, allophane, and immogolite. The two oldest sites, 1400 ka and 4100 ka, are highly weathered Ultisols and Oxisols dominated by relatively inert crystalline Al- and Fe-oxides and kaolin minerals (Chadwick et al., 1999; Vitousek et al., 1997; Pett-Ridge et al., 2007). Furthermore, although quartz and mica in Hawaiian soils are derived uniquely from continental dust sources (Kurtz et al., 2001), only small amounts of mica may be found in the older soil profiles (Ziegler et al., 2005) because dust undergoes chemical weathering in the soil environment older than 150 ka, with mica weathering faster than quartz (Kurtz et al., 2001).

2.2. Sampling and sequential leaching

Soils studied here are the same as those investigated in a companion Li isotope study (Ryu et al., 2014). Samples were collected from hand-dug pits to about 1 m depth except for the youngest soil; Thurston (Th) is about 40 cm deep and overlies unweathered pahoehoe lava, and Ola'a (Ol) is about 70 cm deep and overlies a buried soil on the ~1 ka old Kulanaokuaiki tephra (Fiske et al., 2009; Fig. S1).

In order to distinguish the Mg isotopic composition of different Mg fractions (i.e., labile versus residual Mg) in the soil samples and two USGS reference materials (BHVO-2 and BIR-1), we conducted a three-step leaching and digestion; (1) MilliQ water leach (water leachate), (2) 1 M ammonium chloride (NH_4Cl) leach (NH_4Cl leachate), (3) 4 M acetic acid (HAc) leach (HAc leachate), and (4) complete digestion of the silicate residue (residue).

Steps (1) to (3) define the "labile" Mg, which means the Mg released or exchanged relatively easily when the soil sample is in contact with soil solution. It includes the Mg from the

161 macroporosity (water leachate), the ion-exchangeable Mg (NH_4Cl leachate), and the less
162 leachable Mg in carbonates and/or Fe-oxyhydroxides/silicate lattice (HAc leachate; Jacobson and
163 Blum, 2000; Chan and Hein, 2007; Wimpenny et al., 2014).
164 Step (4) defines the "residual" Mg, which means the Mg mainly associated with the
165 silicate minerals but also (nano)crystalline Fe– and Al–phases.
166
167 *2.3 Sample preparation and elemental analysis*
168 About 1.0 g of the soil samples was reacted with 10 mL of MilliQ water for 6 h using a
169 Thermo Scientific Vari-Mix^{TM} Test Tube Rocker. The mixture was centrifuged, and the
170 supernatant was passed through a 0.45 μm polypropylene syringe filter, dried, and re-dissolved
171 in 5% HNO_3. The residue was then reacted with 10 mL of 1 M NH_4Cl for 6 h (pH = 7) prior to
172 repeating the same procedures above. Thereafter, the residue was reacted with 10 mL of 4 M
173 HAc for 6 h (pH = 2) and repeated the same procedures above. Finally, the residue was dried and
174 a 0.1 g sub-sample was powdered and completely digested in a 5:3 mixture of HF and HNO_3.
175 Bulk soil samples crushed in a shatter box equipped with a tungsten carbide grinding container
176 were also completely digested in a 5:3 mixture of HF and HNO_3. All HF-digested samples were
177 dried, refluxed several times in 6.0 M HCl to remove fluorides, and re-dissolved in 5% HNO_3.
178 Cation and trace element concentrations were measured using a Perkin Elmer Optima 8300 ICP-
179 AES and a Thermo Elemental X-7 ICP-MS, respectively at the Korea Basic Science Institute
180 (KBSI). Repeated analyses of USGS rock standard powders (BCR-2, BHVO-2, and BIR-1)
181 yielded external reproducibilities better than ±5%.
182
183 *2.4. Magnesium isotope analysis*

Magnesium was separated from matrix elements using an AG-50W-X8 resin (200–400 mesh). After loading the sample, matrix elements were eluted with 5 mL of 0.15 M HF, followed by 10 mL of the mixture of 0.5 M HCl and 95% acetone, and 8 mL of 1 M HNO_3 before collecting Mg in 12 mL of 1 M HNO_3. Magnesium isotope ratios were measured using a Neptune MC-ICP-MS upgraded with a large dry interface pump at the KBSI. Samples were introduced using a quartz dual cyclonic spray chamber and analyzed with a standard-sample-standard bracketing method. Sample intensities were matched to within 10% of the intensity of the standard. Using the Jet sample cone and X-skimmer cone, the sensitivity was ~100 V/ppm on mass 24 at a typical uptake rate of 100 μL/min. Prior to isotopic analysis, each sample was checked for yield and the concentration of matrix elements (Al, Ca, Fe, K, Mn, Na, and Ti). Yields were about 100% and the matrix concentration did not exceed 1% of the Mg concentrations. The total procedural blanks were negligible with less than 3 ng of Mg. All $^{26}Mg/^{24}Mg$ and $^{25}Mg/^{24}Mg$ ratios are reported in delta notation relative to DSM-3, where $\delta^{x}Mg = [(^{x}Mg/^{24}Mg)_{sample}/(^{x}Mg/^{24}Mg)_{DSM\text{-}3}-1] \times 1000$ and $x = 25$ or 26. Samples were analyzed in replicate (n = 3 – 4), where uncertainties are reported as two standard deviations (2σ). The long-term Mg isotope measurements of three reference materials (DSM-3, CAM-1, and SRM980) yielded $\delta^{26}Mg$ values of –0.01 ± 0.06‰ (2σ, n = 408), –2.62 ± 0.06‰ (2σ, n = 404), and –4.32 ± 0.09‰ (2σ, n = 249), respectively, in good agreement with reported values (Table S1; e.g., Galy et al., 2001, 2003; Tipper et al., 2008b; Huang et al., 2009; Lee et al., 2014). The chemical purification, and the precision and accuracy of Mg isotope measurements have been validated using the USGS powder and IAPSO seawater reference materials. BHVO-2 yielded a $\delta^{26}Mg$ value of –0.20 ± 0.07‰ (2σ, n = 3), BIR-1 yielded a $\delta^{26}Mg$ value of –0.17 ± 0.08‰ (2σ, n = 4),

and IAPSO yielded a δ^{26}Mg value of –0.83 ± 0.04‰ (2σ, n = 36), consistent with reported values (Table S1; Teng, 2017 and references therein).

2.5. Calculations of Mg gain or loss

The relative gain ($\tau_{j,w} > 0$) or loss ($\tau_{j,w} < 0$) of Mg with depth at each weathering profile was estimated as follows (Brimhall and Dietrich, 1987; Chadwick et al., 1990):

$$\tau_{j,w} = \frac{C_{j,w} \times C_{i,p}}{C_{j,p} \times C_{i,w}} - 1, \quad (1)$$

where *C* is the concentration of an element, *w* and *p* refer to the weathered and parent materials, respectively, and *i* and *j* refer to the immobile and mobile elements, respectively. Kurtz et al. (2000) performed comprehensive analyses of a wide range of trace metals in Hawaiian soils and found that that Nb and Ta are the least mobile elements in these soils compared to traditionally known immobile elements, such as Th, Zr and Al. Thus, for these calculations, we used Nb as the index element.

The depth-integrated τ_{Mg} allows us to calculate the total loss or gain of Mg and other elements over the timescale of each profile as follows:

$$\tau_{int} = \frac{\sum\left(\tau_h \cdot \rho_h \cdot z_h\right)}{\sum\left(\rho_h \cdot z_h\right)}, \quad (2)$$

where τ_h is the $\tau_{j,w}$ value of each horizon (*h*; Eq. (1)), z_h is horizon thickness, and ρ_h is horizon density taken from Pett-Ridge et al. (2007).

2.6. Quantifying relative contribution of each Mg source

Previous work has shown that with age basalt weathering becomes relatively less important to the soil budget and atmospheric inputs become more important, in particular for Sr and Nd (Vitousek et al., 1997; Kurtz et al., 2001; Chadwick et al., 2009). However, a recent study also showed that atmospheric input is not a primary control of Li isotopic compositions in the Hawaiian soils (Ryu et al., 2014). It is possible to estimate the relative contribution from the various Mg sources for each studied soil profile, as has been done for U and Li (Pett-Ridge et al., 2007; Ryu et al., 2014). The Mg contribution from Asian dust can be estimated because the elemental composition of the dust in Hawaii has remained relatively invariant during the past 4100 ka (Kyte et al., 1993). Thus,

$$Mg_{dust} = C_{dust}^{Mg} \cdot F_{dust} \cdot t , \quad (3)$$

where C_{dust}^{Mg} is the average Mg concentration in either upper continental crust (UCC; [Mg] = 1.5 wt.%; Rudnick and Gao, 2014) or in loess ([Mg] = 0.58 wt.%; Li et al., 2010), F_{dust} is the average long-term dust deposition rate for Hawaii (30 mg/cm^2/ka for the younger soils (<20 ka) and 125 mg/cm^2/ka for the older soils (≥20 ka); Kurtz et al., 2001), and *t* is the age of the soil site. Similarly, the atmospheric Mg input linked to rainwater can be calculated as follows:

$$Mg_{rainwater} = C_{rainwater}^{Mg} \cdot MAP \cdot t , \quad (4)$$

where $C_{rainwater}^{Mg}$ is the Mg concentration in Hawaiian rain (5.83×10^{-2} μg/cm^3 at Thurston (Hawai'i) and 1.43×10^{-1} μg/cm^3 at Kokee (Kauai); Carrillo et al., 2002) and *MAP* is the Mean Annual Precipitation (2500 mm/yr). Since the sites exhibit minimal physical erosion, the overall weathering thickness should be directly linked to their age (e.g., Pett-Ridge et al., 2007). In this context, the quantity of Mg released from the parent basalt can be estimated as follows:

$$Mg_{basalt} = C_{basalt}^{Mg} \cdot z_t \cdot S_c \cdot \rho_{basalt} , \quad (5)$$

where C_{basalt}^{Mg} is the Mg concentration in basalt (6.1 wt.% in tholeiitic basalt for the two youngest sites, and 3.3, 2.2, 6.1 and 4.9 wt.% in alkali basalt for the older sites, respectively; Ziegler et al., 2005), z_t is the total regolith thickness (m), ρ_{basalt} is the average density of basalt including void and infilled vesiculated tephra (1.25 g/cm^3; Chadwick et al., 2003), and S_c is the collapse factor. Total regolith thickness is difficult to determine even in cases where a backhoe or drill is available because of local variability related to void spaces and hydrological permeability (Goodfellow et al., 2013). We calculated values representing soil horizons to 1-m depth.

Eqs. (3) – (5) allow us to calculate the total Mg in the regolith, which is the sum of Mg released from the parent basalt, with Mg added from dust and rainwater along the course of the regolith development as follows:

$$Mg_{total} = Mg_{basalt} + Mg_{dust} + Mg_{rainwater}, \quad (6)$$

It is possible to compare Mg_{total} corresponding to the regolith residence time, to the Mg currently present in the regolith, $Mg_{present}$ (i.e. depth-integrated Mg mass per unit area). The difference between these two parameters allows the total Mg exported by the profile Mg_{loss} to be evaluated as follows:

$$Mg_{present} = \sum_h \left(\rho_h \cdot z_h \cdot C_h^{Mg} \right) \quad (7)$$

$$Mg_{loss}\left(\%\right) = \left[Mg_{present} / \left(Mg_{basalt} + Mg_{dust} + Mg_{rainwater} \right) - 1 \right] \times 100, \quad (8)$$

where C_h^{Mg} is the Mg concentration in the each soil horizon. All results are given in Table S3.

3. RESULTS

3.1. Mg concentrations and Mg isotope compositions in bulk soils

Tables 1 and 2 present all Mg isotope data, along with elemental geochemistry reported in Ryu et al. (2014). Magnesium concentrations ([Mg]) of the bulk soil are variable with depth and age, ranging from 0.07 to 8.79 wt.% (Fig. 1). At the 0.3 ka sites (Th and Ol), [Mg] in the organic-rich surface horizons is 0.52 and 1.08 wt.%, respectively, and abruptly increases to about 6.2 wt.% for the deeper horizons, similar to tholeiitic basalt (6.1 wt.%; Ziegler et al., 2005). At the 20 ka site, [Mg] is relatively low for the upper horizons (0.14 wt.% on average; 0−27 cm) and gradually increases to 1.66 wt.% in the deeper horizons (1.66 wt.%; 94−110 cm), which is much lower than that of alkali basalt (2.3 wt.%; Chadwick et al., 2003). At the three oldest sites (150, 1400, and 4100 ka), [Mg] is quite low, ranging from 0.07 to 0.71 wt.%, with an average of 0.25±0.33 wt.% (2σ, n=36).

The δ^{26}Mg values of bulk soil samples span a significant range, from −0.60 to +0.26‰ (−0.16±0.36‰, 2σ, n=36; Table 1 and Fig. 2). The youngest sites (0.3 ka; Th and Ol) exhibit little variation in δ^{26}Mg (−0.27±0.09‰, 2σ, n=13), in good agreement with reported δ^{26}Mg for the Hawaiian basalts (−0.26±0.06‰, 2σ, n=11; Zhong et al., 2017) and for fresh oceanic basalts more generally (−0.26±0.07‰, 2σ, n=110; Teng et al., 2010). At the 20 ka site, δ^{26}Mg values range from −0.44‰ for the organic-rich surface sample to −0.15‰ for the subsurface samples with an average of −0.26±0.26‰ (2σ, n=4). At the 150 ka site, δ^{26}Mg values range from −0.60‰ for the organic-rich surface sample to −0.01‰ for the subsurface samples with an average of −0.12±0.47‰ (2σ, n=6). At the 1400 ka site, δ^{26}Mg value is the lowest at the organic-rich surface (−0.55‰), and increases up to 0.26‰ for the subsurface samples with an average of −0.04±0.54‰ (2σ, n=6). At the oldest site (4100 ka), δ^{26}Mg values are relatively consistent, ranging from −0.11 to +0.05‰, with an average −0.05±0.13‰ (2σ, n=6), regardless of depth.

292 *3.2. Mg isotope compositions in sequential leachates and residue*

293 In the various leachates, Mg displays a wide range of δ^{26}Mg values, from −1.01 to
294 +0.06‰ (−0.37±0.53‰, 2σ, n=58; Table 2 and Fig. 2). The water and NH_4Cl leachates have
295 similar δ^{26}Mg values, within uncertainty, of −0.37±0.53‰ (2σ, n=23) and −0.28±0.49‰ (2σ,
296 n=14), respectively, The HAc leachate displays relatively lighter δ^{26}Mg values of −0.42±0.53‰
297 (2σ, n=21). The residual Mg, With the exception of the organic-rich surface samples, residual
298 Mg at the sites older than 20 ka, showed much heavier δ^{26}Mg values of +0.02±0.48‰ (2σ, n=25)
299 (Table 2). We define a "labile" pool as the sum of Mg released during the water, NH_4Cl and HAc
300 leaches, which shows that the two youngest sites (0.3 ka; Th and Ol), display a labile Mg with an
301 average δ^{26}Mg value of −0.18±0.13‰, (2σ, n=31). The residues ('residual' Mg) show an average
302 δ^{26}Mg value of −0.23±0.05‰ (2σ, n=11) that is consistent with Hawaiian basalt within
303 uncertainties.

304 In contrast, at the 20 ka site, the 'labile' Mg in the organic-rich surface sample becomes
305 depleted in heavy Mg isotopes (−0.49±0.23‰, 2σ, n=3) compared to the residual Mg (−0.07‰,
306 n=1). In the subsurface samples of the same site, both labile and residual Mg display similar
307 δ^{26}Mg values of −0.01±0.21‰ (2σ, n=2) and −0.03±0.08‰ (2σ, n=3), respectively.

308 Interestingly, at the sites older than 20 ka, the labile Mg from the organic-rich surface
309 samples display much lighter δ^{26}Mg values (−0.59±0.31‰, 2σ, n=15) compared to basalts. For
310 the subsurface samples at the sites older than 150 ka, the residual Mg becomes enriched in heavy
311 Mg isotopes (+0.24±0.24‰, 2σ, n=13) compared to the labile Mg (−0.59±0.31‰, 2σ, n=15).

312

313 **4. DISCUSSION**

314 *4.1. Variations of Mg concentrations in soils*

315 Figure 1 shows the depth variations of [Mg] in all soil profiles. In the organic-rich surface
316 horizons, τ_{Mg} decreases from −18% to −99% with age, indicating progressive loss of Mg during
317 pedogenesis. In the two youngest soils, the organic-rich surface is already depleted by up to 29%
318 in Mg compared to parent basalt. This could be partly explained by the dilution by soil organic
319 matter (SOM) due to the high SOM content of the 0–3 cm depth sample (56 wt.%) (Ziegler et al.,
320 2005). Another possibility is that Mg released from basalt leaching and/or from decomposition of
321 plant would move deeper into the profile or be lost because Mg is highly mobile and water-
322 soluble. Below 12 cm depth in the two youngest soils (0.3 ka), τ_{Mg} turns into positive, indicating
323 the enrichment relative to the surface and the relative gain of Mg compared to basalt. This
324 feature is likely the result of the surface Mg moving deeper into the profile. At the sites older
325 than 0.3 ka, τ_{Mg} abruptly decreased near −100% compared to the 0.3 ka sites due to the
326 significant consumption of primary minerals by 20 ka (Vitousek et al., 1997). In contrast, both
327 [Al] and [Fe] increase with depth as well as age (Fig. 1) due to residual enrichment and
328 redistributions. These metals are more strongly retained during progressive mineral
329 transformations starting with the synthesis of metastable SRO minerals and followed by their
330 transformation into relatively inert secondary minerals. Although SRO minerals (e.g., allophane,
331 imogolite and ferrihydrite) and sesquioxides (hematite and goethite) replaced primary minerals
332 during the first 20 ka (Chorover et al., 1999) with large specific surface areas of 600 m^2/g (Hall
333 et al., 1985) and 120 m^2/g (Schwertmann and Taylor, 1989), respectively, only a little Mg was
334 trapped within aggregates formed by association of SRO and organic matter (Opfergelt et al.,
335 2014). At the three older sites (150, 1400 and 4100 ka), τ_{Mg} is close to −100% at all depths
336 although the contents of poorly crystalline total (gibbsite and poorly crystalline kaolin minerals)

and kaolin minerals (kaolinite and halloysite) significantly increase (Ziegler et al., 2005). Overall, most of Mg released from basalt leaching was lost (up to 100%) in the soils older than 0.3 ka and only a small amount of the remaining Mg was either trapped within aggregates formed by association of secondary phases and organic matter (Opfergelt et al., 2014) or incorporated into the octahedral sites of secondary phases.

Depth-integrated τ_{Mg} (τ_{int}^{Mg}) values allow us to investigate the variations of Mg along the LSAG (Fig. 3). As previously described in Ryu et al. (2014), τ_{int} for alkali elements (Na and K) are negative at all sites and the older soils (≥20 ka) display average τ_{int} of close to −100%, indicating that both Na and K are completely lost after 20 ka (Vitousek et al., 1997). In contrast, τ_{int} for alkaline earth elements (Sr and Mg) are positive at the two youngest sites (0.3 ka). Interestingly, at the 20 ka site τ_{int}^{Mg} is relatively high compared to Na, K, and Sr, similar to τ_{int}^{Li} (Ryu et al., 2014). This relatively high τ_{int}^{Mg} relative to Na, K and Sr at the 20 ka could be due to the fact that the surface 25 cm was deposited by renewed eruptions about 5 ka at the 20 ka site (Chadwick et al., 2009) and/or to the lower mobility of Mg (compared to alkali elements) during mineral leaching. For the older sites (≥150 ka), τ_{int}^{Mg} is close to −100%, indicating that secondary phases do not retain Mg during neoformation, in contrast to Li which was significantly retained by crystalline phases (e.g., kaolin minerals; Ryu et al., 2014). Previous studies showed that gibbsite and kaolinite contain small amount of Mg (typically <~ 0.02 wt.%) (Peskleway et al., 2003; Mermut and Cano, 2001).

Previous works have shown that with age basalt leaching becomes relatively less important to the soil budget for several elements, such as Sr and Si, and atmospheric inputs (dust and rainwater) become more important (Kurtz et al., 2001; Ziegler et al., 2005; Chadwick et al.,

2009). However, a recent Li isotope study showed that the relative proportion of each Li source (basalt, dust and precipitation) is 80−100%, 6−20%, and 0.8%, respectively (Ryu et al., 2014), indicating a major contribution of basalt weathering to the Li budget that is significantly retained in secondary phases, in particular in kaolin minerals (kaolinite and halloysite). Using Eqs. (3) – (8) above, we calculated the contribution of each Mg source to the soil Mg budget and Mg loss (Fig. S2 and Table S3). The results show that the parent basalt provided between 78% and 100% of Mg_{total} and dust becomes significant from 150 ka (6%) and reached at maximum 22% of Mg_{total} at 4100 ka. It is interesting to note that although the impact of dust input on the Sr budget is significant at 150 ka (Stewart et al., 2001), it is not the case in the Mg budget because dust is highly depleted in Mg compared to basalt (Kurtz et al., 2001), and because most of Mg at the older sites (≥20 ka) are lost due to weathering, dissolution and leaching by soil waters (Table S3).

4.2. Magnesium isotopic compositions of 'labile' Mg

A sequential leaching of USGS reference materials (BHVO-2 and BIR-1) showed that water leachate yielded lighter $\delta^{26}Mg$ values compared to the other leachates, indicating water-soluble Mg is depleted in heavy Mg isotopes (Table S1). However, as shown in section 3.2, Hawaiian soil samples showed that the water and NH_4Cl leachates have similar $\delta^{26}Mg$ values, of which the 0.3 ka site samples have $\delta^{26}Mg$ values of −0.20±0.11‰ (2σ, n=9) and −0.11±0.11‰ (2σ, n=7), respectively. Although it is difficult to compare them to soil samples older than 20 ka due to a limited data, both leachates also show similar $\delta^{26}Mg$ values within uncertainties (Table 2). This result is consistent with previous work showing that water and exchangeable fractions have similar isotopic compositions for Ca, Sr, and Ba isotope systems (Bullen and Chadwick,

382 2016). Thus, the water and NH_4Cl leachates together are hereafter referred to 'exchangeable
383 Mg'. Previous studies have shown that exchangeable Mg in volcanic soils (Opfergelt et al.,
384 2014), clay minerals (Wimpenny et al., 2014) and paddy soils (Gao et al., 2018) leached by
385 either NH_4Ac or NH_4Cl are depleted in heavy Mg isotopes compared to bulk samples, suggesting
386 that the isotopic composition of exchangeable Mg is likely to reflect either the fluid phases in
387 which the sample last equilibrated (Wimpenny et al., 2014; Gao et al., 2018) or the mixture of
388 different Mg sources (sea spray and organic matter) as well as the possible effects of sorption
389 (Opfergelt et al., 2014). However, exchangeable Mg in the Hawaiian soil samples are enriched in
390 either heavy Mg isotopes at the 0.3 ka sites or depleted at the sites older than 20 ka. We will
391 discuss the processes controlling the isotopic composition of exchangeable Mg in a later section.
392 The HAc leachates have Mg isotopic composition either similar to or a bit more depleted
393 in heavy Mg isotopes compared to exchangeable Mg, of which the 0.3 ka site samples have
394 δ^{26}Mg value of −0.18±0.09‰ (2σ, n=9) and the samples at the older sites (≥ 20 ka) have δ^{26}Mg
395 value of −0.67±0.35‰ (2σ, n=9). However, a previous study found that the HAc leachates from
396 clay minerals were relatively enriched in heavy Mg isotopes (Wimpenny et al., 2014), suggesting
397 that while the HAc leach mostly accounts for either ion-exchangeable Mg, it may also remove
398 other easily leachable phases (carbonates or Fe-oxyhydroxides; Jacobson and Blum, 2000; Chan
399 and Hein, 2007) or cause some breakdown of the mineral lattice (Jacobson and Blum, 2000).
400 Because the Hawaiian soils we sampled contain no pedogenic carbonates (Vitousek et al., 1997;
401 Chadwick et al., 2009; Ziegler et al., 2005), the Mg isotopic composition of the HAc leachates
402 would reflect less labile, more strongly bound Mg onto either surface complexes of secondary
403 phase (SRO) and soil organic matter (SOM) and/or Fe-oxyhydroxides. We will discuss the
404 processes controlling the isotopic composition of Mg from HAc leachates in a later section.

405

406 *4.2.1. Behavior of Mg isotopes in the organic-rich surface soil*

407 Although simple mass balance indicates that the contribution of basalt weathering to the
408 soil Mg budget is dominant, the contribution of other sources, such as dust, rainwater and plants,
409 on Mg isotopic compositions in the surface samples (O horizon; < 6 cm except for 20 ka site)
410 could be significant because [Mg] is quite depleted (Fig. 1). Figure 4a shows Mg isotope
411 variations in the organic-rich surface soil as a function of age. The δ^{26}Mg values of 'labile' Mg
412 (released by water, NH_4Cl and HAc leach, as explained in section 2.2) in the surface samples
413 range from −0.88±0.24‰ (2σ, n=3) at the 150 ka site to −0.23±0.13‰ (2σ, n=6) at the 0.3 ka
414 sites. The HAc leachates display much lighter δ^{26}Mg values at the sites older than 0.3 ka (Table
415 2). Although the 'labile' Mg is depleted in light Mg isotopes, previous studies have shown that
416 labile Mg can be isotopically depleted (Opfergelt et al., 2012; Wimpenny et al., 2014) or
417 enriched in heavy Mg isotopes (Huang et al., 2012; Pogge Von Strandmann et al., 2012). At the
418 0.3 ka sites, δ^{26}Mg values of all labile Mg are similar to that of Hawaiian basalt within errors.
419 Because Mg is an essential nutrient for plant growth, plants play an important role of its
420 recycling in the soil system, especially at the surface, as plants take up and release Mg during the
421 growth and decay, respectively. Both the organic-rich surface soils and labile fractions showed
422 an enrichment of K relative to Na, when compared to K/Na ratios of basalt (0.24-0.39; Ziegler et
423 al., 2005) and rainfall (0.05-0.18; Bern et al., 2015), suggesting that vegetation is transporting
424 biologically important elements to the surface (since Hawaiian plants have highly enriched K/Na
425 ratios (Trostle, 2014)). Plants preferentially accumulate heavy Mg isotopes in their tissues,
426 resulting in soil water depleted in heavy Mg isotopes (Black et al., 2008; Bolou-Bi et al., 2010,
427 2012). Since we did not detect Mg isotope fractionation of the 'labile' Mg in the O horizon at the

two youngest sites, we suspect that biological fractionation is being masked by the high Mg supply from congruent basalt weathering. In addition, these young soils only a small amount of the primary minerals have transformed to secondary clays (e.g., Chorover et al., 2004; Ziegler et al., 2005); as a consequence, the residual Mg displays a δ^{26}Mg value of −0.20±0.01‰ (2σ, n=2) similar to Hawaiian basalt.

At the older sites (>0.3 ka), δ^{26}Mg values of labile Mg in the organic-rich surface samples decrease from −0.49±0.23‰ (2σ, n=3) to −0.70±0.24‰ (2σ, n=2) with age (Fig. 4a). The HAc leachates display lower δ^{26}Mg values than both water and NH_4Cl leachates (i.e., exchangeable Mg). This suggests that less labile Mg strongly bound onto either the complexes of secondary phase and soil organic matter (SOM) and/or Fe-oxyhydroxides is depleted in heavy Mg isotopes. At the sites older than 20 ka, δ^{26}Mg values of the 'labile' Mg is variable, of which water-soluble Mg yields δ^{26}Mg values similar to that of seawater (−0.83±0.09‰, 2σ; Ling et al., 2011). This suggests substantial contribution of dilute rainwater Mg to this labile pool. Nonetheless, we could not exclude the effect of plant biocycling of Mg because both plant uptake and secondary mineral formation causes soil water to be depleted in isotopically heavy Mg. On the other hand, δ^{26}Mg values of residual Mg in the surface samples are quite variable, ranging from −0.44 to +0.19‰. All these surface samples mainly contain SOM with little secondary phases (Table S2; Ziegler et al., 2005). Previous studies have shown that the top 5 cm of the soil profiles exhibit a shift toward more negative δ^{30}Si values due to plant-related Si uptake and phytolith precipitation (recycled biogenic silica) in the topsoil (Derry et al., 2005; Ziegler et al., 2005). Likewise, a shift toward more positive δ^{26}Mg values in the organic-rich surface samples is likely to be plant-related Mg uptake and litterfall decomposition. Indeed, previous studies have shown that plants (e.g., particularly roots (Bolou-Bi et al., 2012) and aboveground vegetation (Trostle, 2014)) can

451 be enriched in heavy Mg isotopes. However, more investigations are needed to confirm it in the
452 case of these Hawaiian ecosystems.
453
454 *4.2.2. The impact of vegetation on the labile Mg*
455 At the two youngest sites, the 'labile' Mg of the subsurface soils display δ^{26}Mg values
456 ranging from −0.29 to −0.02‰, with an average of −0.17±0.12‰ (2σ, n=25). Furthermore, the
457 water, NH_4Cl and HAc leachates have similar average δ^{26}Mg values of −0.20‰, −0.11‰, and
458 −0.18‰, respectively (Table 2). The fact that all the leachates are close to the Hawaiian basalts
459 is likely due to the large concentration of Mg supplied by congruent basalt weathering, which
460 buffers the effect of Mg isotope fractionation by plants. An alternative is that the degree of Mg
461 isotope fractionation by Hawaiian plants may not be as large as what is known for
462 granite/sandstone-grown plants (Bolou-Bi et al., 2012), but we consider this explanation unlikely
463 because hydroponic experimental approaches and adsorption on organics also demonstrated
464 strong isotope fractionations (up to +1.66‰; Bolou-Bi et al., 2010, 2012; Black et al., 2008).
465 At the 20 ka site, water leachates of two subsurface samples have average δ^{26}Mg value of
466 −0.01±0.21‰ (2σ, n=2), ranging from −0.08 to +0.06‰. This indicates that the solution (i.e.,
467 soil water) is enriched in isotopically heavy Mg compared to Hawaiian basalt or rainwater (Fig. 4
468 and Table 2) and therefore a simple mixing of these two sources (basalt dissolution and rain)
469 cannot explain the isotopic values. In contrast, it has been shown that litterfall supplies organic
470 matter that is a key constituent of the soil exchange complex and thus a potential sink for Mg
471 (Bolou-Bi et al., 2010, 2012; Opfergelt et al., 2014). Therefore, these results suggest that, since
472 litter decomposition could significantly affect the Mg biogeochemical cycle, it could also explain

473 the shift towards heavy δ^{26}Mg of the exchangeable or labile fraction (Bolou-Bi et al., 2012;
474 Opfergelt et al., 2014).

475 At the older sites (≥20ka), despite limited data, Mg isotope variations of the labile pool
476 are similar to the ones observed in the O horizon, as discussed above (Fig. 4). The δ^{26}Mg values
477 of the 'labile' Mg range from −0.89 to +0.06‰, with an average of −0.52±0.49‰ (2σ, n=17;
478 Table 2). The water and NH_4Cl leachates (exchangeable Mg) have average δ^{26}Mg value of
479 −0.45±0.56‰ (2σ, n=10), slightly heavier than the HAc leachate (−0.63±0.28‰, 2σ, n=7). This
480 is much heavier than local rainwater and therefore these variations can also be partly attributed to
481 downward migration of dissolved organic matter and the plant-related Mg redistribution (Figs. 4
482 and 5), as evidenced in previous studies (e.g. Marin-Spiotta et al., 2011; Kramer et al., 2012;
483 Bullen and Chadwick, 2016). Furthermore, it cannot be explained by the mixing between local
484 rainwater and congruent dissolution of basalt because primary minerals were completely
485 consumed before 20 ka (Vitousek et al., 1997; Kennedy et al., 1998). It is possible that Mg
486 isotope variations of the labile Mg at the older sites (≥20ka) may reflect the plant-related Mg
487 recycling of different tissues of plants with different Mg isotopic compositions (Bolou-Bi et al.,
488 2012). Indeed, plants drawing upon high levels of available nutrients in fertile sites (young- to
489 intermediate-aged sites) produce tissues with relatively high nutrient concentration and
490 decompose more rapidly than those from infertile sites (older sites; Vitousek et al., 1997); This
491 was shown for Ca isotopes (Wiegand et al., 2005). Further investigations are needed to quantify
492 more precisely Mg isotope fractionation by biological Mg recycling in the soil system, but this
493 study indicates that when the concentration of Mg is relatively low due to little basalt weathering
494 input, the isotopic composition of labile Mg is more likely to be influenced by plant-related Mg
495 recycling rather than local rainwater.

496

497 *4.3. Different behavior of Mg isotopes in the residual Mg*

498 Contrary to labile Mg, most of residual Mg plotted outside of a mixing plot, indicating
499 other processes, such as basalt weathering and secondary phase formation, may control their Mg
500 isotopic compositions (Fig. 5). In following sections, we discuss the mechanisms involved in
501 setting the isotopic signal in the residual Mg.

502

503 *4.3.1. Basalt weathering*

504 We don't fully understand the controls on Mg isotope fractionation during weathering.
505 Two experimental studies have concluded that silicate dissolution causes dissolved phases to
506 have different Mg isotope composition compared to parent mineral/rock due to either isotope
507 fractionation or conservative mixing (Wimpenny et al., 2010; Ryu et al., 2011, 2016). For the
508 Hawaiian LSAG sites, other isotope systems, such as Si and Li isotopes (Ziegler et al., 2005;
509 Ryu et al., 2014), have revealed that basalt leaching does not fractionate those isotopes at the 0.3
510 ka sites. Therefore, the behavior of Mg isotopes at the two youngest sites provide a baseline for
511 evaluating Mg isotope fractionation during progressive basalt dissolution. For subsurface
512 samples at the 0.3 ka sites, the differences in δ^{26}Mg values between all labile Mg and bulk basalt
513 ($\Delta^{26}Mg_{\text{labile Mg–basalt}}$) range from –0.02 to +0.25‰, with an average of +0.10±0.15‰ (2σ, n=13) at
514 the Th site and of +0.10±0.09‰ (2σ, n=12) at the Ol site (Table 2 and Fig. 4b). Likewise,
515 $\Delta^{26}Mg_{\text{residual Mg–basalt}}$ ranges from 0.00 to +0.07‰, with an average of +0.04±0.04‰ (2σ, n=5) at
516 the Th site and of +0.04±0.06‰ (2σ, n=4) at the Ol site. Although labile Mg has a slightly heavy
517 δ^{26}Mg value compared to bulk basalt, all results highlight that basalt weathering does not
518 fractionate Mg isotopes. Secondary mineral phases in these soils (up to 18 wt.% of SRO minerals

519 and 13 wt.% of poorly crystalline; Ziegler et al., 2005) have little effect on Mg isotopic
520 compositions of both labile and residual Mg, which seem to be set by the basalt isotopic
521 signature. In short, no difference in δ^{26}Mg values between soil and basalt at the two youngest
522 sites confirms that Mg isotope fractionation is negligible during basalt weathering under natural
523 conditions. Fractionation processes are imposed by soil and ecosystem processes acting on the
524 Mg once it is released from rock minerals.
525
526 *4.3.2. Secondary mineral formation*
527 As elements are being leached from basalt, the remaining element configurations become
528 more stable: soil minerals evolve first to SRO minerals (e.g., allophane and ferrihydrite),
529 sesquioxides (hematite and goethite), and then to crystalline products, such as goethite, gibbsite
530 and kaolin minerals (Vitousek et al., 1997; Chorover et al. 2004; Ziegler et al., 2005). To date,
531 although many experimental and field studies have investigated Mg isotope fractionation during
532 secondary mineral formation, the reported directions are not yet clear (e.g., Wimpenny et al.,
533 2010, 2014; Huang et al., 2012; Liu et al., 2014; Opfergelt et al., 2014; Ryu et al., 2016; Gao et
534 al., 2018; Hindshaw et al., 2020). As detailed below, our results for the Hawaiian soils are
535 consistent with enrichments in heavy isotopes during secondary phases formation.
536 First, at the 20 ka site, the soils contain mostly SOM, chemically active SRO minerals
537 (allophane and ferrihydrite) and sesquioxide phases (goethite and hematite), in which SRO
538 minerals combined with SOM could adsorb labile Mg onto their surfaces (Chorover et al., 2004),
539 implying that the complexes of SRO minerals combined with SOM control the Mg retention
540 capacity on the soil exchange complex. As discussed in section 4.4.2, the two water leachates
541 significantly enriched in heavy Mg isotopes (−0.01±0.21‰, 2σ, n=2) compared to Hawaiian

basalt or rainwater likely reflect plant recycling. However, we cannot exclude the possibility that Mg isotope fractionation occurred during adsorption onto oxides – we did not conduct Mg isotope sorption experiments to evaluate that possibility. Furthermore, residual Mg in the subsurface samples at the 20 ka site showed much heavier δ^{26}Mg values of −0.03±0.08‰ (2σ, n=3) compared to bulk basalt (Figs. 2c & 4b and Table 2). Although Opfergelt et al. (2014) suggested that Mg cannot be easily incorporated into the octahedral sites of SRO minerals (allophane), other studies showed that Mg in the SRO extraction through the treatment with oxalate in the dry soils on Kohala displayed much heavier δ^{26}Mg values compared to Hawaiian basalt (Trostle, 2014) and that δ^{26}Mg in bauxites correlates with gibbsite abundance (Liu et al., 2014), indicating that either nanocrystalline (SRO) and/or crystalline Fe– and Al–phases (i.e. goethite/hematite and gibbsite) may be responsible for enriched heavy Mg isotopes in residual Mg. Changes in bond lengths and vibrational frequencies in the octahedral sheets affect isotope fractionation (Wang et al., 2017) as the crystal structure distorts to accommodate an ion with a different charge and/or radius (Laurora et al., 2011; Michalski et al., 2015). Therefore, during the substitution of octahedrally coordinated Fe by Mg in goethite/hematite, the bond length from substituting elements can be approximated as the sum of the ionic radii of the cation and of the 6-fold coordination O^{2-} anion (Shannon, 1976) even if bond lengths are not always accurately known. For example, because the ionic radii of octahedral Mg^{2+} (0.72 Å) and Fe^{3+} (0.645 Å) are slightly different (Shannon, 1976), the average Mg–O bond length in goethite (~2.095 Å) is longer than the average Fe–O bond length (~2.02 Å; Changela et al., 2012) through cation substitution, which is also longer than the average Mg–O bond length in water (~2.07 Å; Carugo et al., 1993; Bock et al., 1994; Pavlov et al., 1998). Likewise, gibbsite has two-thirds of its octahedral sites filled with Al^{3+} and one-third unoccupied, allowing small cations (e.g., Li, Mg,

565 Ni and Co) to fit into the unoccupied octahedral voids without significant deformation of the
566 layer (Isupov, 1999). As we discussed above, the intercalated Mg–O length in gibbsite (2.105 Å)
567 is longer than the Al–O length in gibbsite (1.92 Å; Ladeira et al., 2001) or the average Mg–O
568 bond length in water (2.072 Å) without substantial bond contraction (Isupov, 1999). Although
569 several studies proposed a general trend relating Mg–O bond length to the direction of Mg
570 isotope fractionation (e.g., Liu et al., 2014; Gao et al., 2018; Hindshaw et al., 2020), there does
571 not appear to be a strong correlation between average Mg–O bond length and Mg isotope
572 fractionation in octahedral coordination (Schauble, 2011). Therefore, the fact that residual Mg is
573 enriched in heavy Mg isotopes is more likely to attributed to nanocrystalline (SRO) Fe– and Al–
574 phases rather than gibbsite although this would certainly deserve to be verified experimentally.
575 Contrary to the 20 ka site, the 150 ka soils at depth of < 30 cm contain large amounts of
576 Qtz and mica (depth-integrated τ_{int} = 15 wt.%; Ziegler et al., 2005), indicating significant impact
577 of dust input. The impact for Mg may be smaller because a) basalts have high initial Mg contents
578 and b) the isotopic contrast between radiogenic continental Sr and basaltic Sr is greater than
579 between dust and basalt sources which have similar δ^{26}Mg values. If Asian dust has strongly
580 influenced samples, the soil samples should reflect Mg isotopic composition of Asian dust (Fig.
581 5). Previous studies indicated that the average composition of Asian dust delivered to Hawaii has
582 not varied over the last 4 million years spanning the Hawaii chronosequence (Kyte et al., 1993),
583 and that modern Asian dust largely reflects the average composition of upper continental crust
584 (UCC; Zieman et al., 1995). Furthermore, the fact that the difference in a weighted average
585 δ^{26}Mg between the UCC (–0.22‰; Li et al., 2010) and 20 sedimentary composites from eastern
586 China (–0.16‰; Li et al., 2010) is within the analytical error of ±0.1‰ (2σ) indicates that Mg
587 isotopic composition of Asian dust reflects that of UCC. Nonetheless, residual Mg in the

588 subsurface samples yield a δ^{26}Mg value of +0.18±0.18‰ (2σ, n=4) much heavier than both
589 Hawaiian basalt and UCC (Figs. 2d & 4b). Instead, the subsurface soils also contain greater
590 amounts of chemically active SRO minerals, Fe– and Al–crystalline compounds, and poorly
591 crystalline kaolin minerals (Chadwick et al., 2003; Chorover et al., 2004; Ziegler et al., 2005). As
592 discussed above, the incorporation of Mg into both SRO and Fe– and Al–crystalline phases
593 causes residual Mg to be enriched in heavy Mg isotopes at the 150 ka site as well.
594 At the 1400 ka site, the subsurface soil samples mainly contain SRO minerals and
595 crystalline phases (i.e., gibbsite and kaolinite/halloysite; Chorover et al., 2004; Ziegler et al.,
596 2005). For the subsurface soil samples, the residual Mg showed δ^{26}Mg values ranging from
597 +0.27 to +0.46‰, with an average of +0.38±0.18‰ (2σ, n=4), much heavier than basalts and
598 other younger sites (Figs. 2e & 4b). This implies that the incorporation of Mg into the octahedral
599 sites of crystalline secondary minerals (i.e., kaolinite/halloysite) plays a key role, and that this
600 process favors an isotope fractionation towards heavy Mg isotopes (Fig. 5b). As discussed above,
601 Mg could be incorporated into the octahedral sites of kaolinite/halloysite substituting for Al
602 because kaolinite/halloysite is a 1:1 continuous layered silicate composed of an octahedral layer
603 coordinated to a tetrahedral layer similar to lizardite (Ryu et al., 2016). Considering the Al–O
604 length in kaolinite (~1.91 Å; Bish, 1993), the incorporated Mg–O length in kaolinite (~2.095 Å)
605 is longer than the average Mg–O length in water (~2.07 Å; Carugo et al., 1993; Bock et al.,
606 1994; Pavlov et al., 1998) due to the ionic radii of Mg^{2+} (0.72 Å) and Al^{3+} (0.535 Å; Shannon,
607 1976). However, experimental study showed that the residual kaolinite is enriched in heavy Mg
608 isotopes compared to bulk kaolinite (+1.63‰; Wimpenny et al., 2014), implying that it is
609 difficult to relate Mg–O bond length to the direction of Mg isotope fractionation when the
610 difference in bond length between two phases is small, and that the direction of Mg isotope

611 fractionation could be dependent on local field conditions (Hindshaw et al., 2020). In short,
612 positive δ^{26}Mg values of residual Mg in soil at the 1400 ka site likely reflect additional Mg
613 isotope fractionation caused by kaolinite/halloysite formation.

614 At the oldest-aged site (4100 ka), the subsurface soil samples mainly contain Al- and Fe-
615 crystalline compounds and crystalline kaolin minerals (i.e. goethite/hematite, gibbsite, and
616 kaolinite/halloysite) (Chorover et al., 2004; Ziegler et al., 2005). For the subsurface soil samples,
617 the residual Mg showed heavy δ^{26}Mg values ranging from +0.13 to +0.26‰, with an average of
618 +0.18±0.10‰ (2σ, n=5), evidencing that crystalline secondary phases (i.e. goethite, gibbsite and
619 kaolinite/halloysite) preferentially incorporate heavy Mg isotopes into their octahedral sites,
620 causing Mg isotope fractionation (Figs. 2f & 4b). Previous Li isotope study suggested that
621 warmer and wetter conditions in the Pliocene enhance more congruent release of Li isotopes
622 during periods of more intensive weathering of the basaltic rocks (Ryu et al., 2014). Likewise,
623 this process may explain the 4100 ka soils have relatively lighter δ^{26}Mg compared to the 1400 ka
624 soils. Otherwise, gibbsite may lead to larger Mg isotope fractionation rather than kaolinite
625 because 1400 ka soils contain more gibbsite than 4100 ka soils (Ziegler et al., 2005), but this
626 remains to be rigorously demonstrated.

627 Overall, based on our dataset, δ^{26}Mg values at sites older than 20 ka would be controlled
628 mainly by Mg isotope fractionation through crystallographical evolution from Fe– and Al–
629 crystalline compounds (i.e., goethite/hematite and gibbsite) to kaolin minerals (kaolinite and
630 halloysite). Although it is not possible to quantitatively estimate the degree of Mg isotope
631 fractionation during basalt weathering and secondary minerals transformations in the Hawaiian
632 chronosequence, it appears that crystalline secondary phases preferentially incorporate heavy Mg
633 isotopes during their transformations, confirming the close relation between the Mg–O bond

length and the direction of Mg isotope fractionation (Hindshaw et al., 2020). Furthermore, the results indicate that the degree of Mg isotope fractionation is mainly attributed to secondary mineral transformations as a function of soil age.

4.4. Comparison with other studies

The LSAG has been very well-studied in several isotope systems, such as Ca, Si, Li isotopes (Wiegand et al., 2005; Ziegler et al., 2005; Ryu et al., 2014; Bullen and Chadwick, 2016) in order to decipher biogeochemical processes involved in the terrestrial element cycle, and highlight the role of basalt weathering and secondary mineral transformation. In particular, Wiegand et al. (2005) examined $^{87}Sr/^{86}Sr$ ratios and Ca isotopes along the LSAG to see how different alkaline earth elements behave, highlighting the effects of both marine aerosol and plant cycling on Ca isotopes. As shown for [Mg] and its isotopic composition of labile Mg in this study, they indicated that both exchangeable and total Ca pool decrease with age and that Ca isotopes in soil exchangeable pool are influenced by the mixture of marine aerosol and plant-related Ca cycling. Likewise, Bullen and Chadwick (2016) analyzed Ba, Ca and Sr stable isotopes along the Kohala climosequence and found that biocycling of these ions created a negative fractionation that was maintained on the near-surface exchange complex, although with differing affinities – Ba was most strongly held and Ca least strongly held against leaching. Overall, stable isotope systems of alkaline earth elements can be powerful proxies for deciphering their biogeochemical cycles.

As a relevant study, Trostle et al. (2014) investigated Mg isotopes at an arid (~30 cm MAP) soil chronosequence on the Island of Hawaii and highlighted the contribution of pedogenic carbonate to light Mg isotopes in soils. Furthermore, they suggested that the evolution

of the soil mineralogy and morphology during progressive soil development results in significant changes in Mg isotopes through time, which is consistent with our study. Although there is little effect of pedogenic carbonates on the isotopic composition of Mg in this study, both studies indicate that basalt weathering and secondary mineral transformation plays an important role of Mg isotopic compositions in soil system with little effect of Asian dust, incorporating heavy Mg isotopes into secondary phases. However, when compare the Mg isotope study conducted in Iceland (Opfergelt et al., 2014) to our study that both are basaltic soil but different climate, there are clear discrepancies between them. Opfergelt et al. (2014) showed that both exchangeable Mg and clay fractions are depleted in heavy Mg isotopes compared to basalt although bulk soils are isotopically similar to the parent basalt, highlighting the importance of Mg retention on the soil exchange complex and the contribution of sea spray and vegetation (Fig. 5). While the soil exchange complex is a key factor controlling Mg isotopes in both soil systems, in Iceland cold conditions lead to slower weathering rates and development of crystalline secondary phases, whereas in Hawaii there is fast secondary mineral transformation that enhances incorporation of isotopically heavy Mg into crystalline secondary phases.

5. CONCLUSIONS

The Hawaiian Islands LSAG chronosequence allows us to better understand Mg isotope fractionation during progressive basalt weathering and open-system biogeochemical transformations in soil. Given the large concentration of Mg in basalts, the effect of atmospheric deposition to the soil Mg budget for all the sites is small. The major fractionations to Mg isotopes in soils are strong plant-related changes to labile Mg, although there may be some effect due to rainwater input and bond-length selectivities during incorporation of Mg into secondary

Al– and Fe–oxyhydroxides. The variations of Mg isotopes in residual Mg mostly reveal Mg isotope fractionation during secondary mineral formation favoring heavy Mg isotopes. Two youngest soils (0.3 ka; Th and Ol) display δ^{26}Mg values consistent with Hawaiian basalt, regardless of labile and residual Mg, indicating that basalt weathering results in little or no Mg isotope fractionation over 0.3 ka. However, residual Mg in the intermediate- and oldest-soils (≥ 20 ka) display more variable but much enriched δ^{26}Mg values compatible with the known mineralogical and crystallographical evolution of these profiles, suggesting that secondary mineral transformation is a key process controlling Mg isotope fractionation. Overall, Mg isotope variations in labile and residual Mg of soils in Hawaiian LSAG are determined by the effects of plant-related Mg recycling and incorporation of heavy Mg isotopes into (nano)crystalline secondary phases.

ACKNOWLEDGMENTS

This work was supported by the National Research Foundation of Korea (NRF) grants funded by the Korea government (MSIT) (No. NRF-2019R1A2C2085973).

REFERENCES

Bern C.R., Chadwick O.A., Kendall C. and Pribil M.J. (2015) Steep spatial gradients of volcanic and marine sulfur in Hawaiian rainfall and ecosystems. *Sci. Total Environ.* **514**, 250-260.

Berner R.A., Lasaga A.C. and Garrels R.M. (1983) The carbonate–silicate geochemical cycle and its effect on atmospheric carbon dioxide over the past 100 million years. *Am. J. Sci.* **283**, 641–683.

Berner R.A. (2004) *The Phanerozoic Carbon Cycle: CO_2 and O_2*. Oxford University Press.

Bish D.L. (1993) Rietveld refinement of the kaolinite structure at 1.5 K. *Clays Clay Miner.* **41**, 738–744.

Black J. R., Epstein E., Rains W. D., Yin Q. Z. and Casey W. H. (2008) Magnesium-isotope fractionation during plant growth. *Environ. Sci. Technol.* **42**, 7831–7836.

Bock C.W., Kaufman A. and Glusker J.P. (1994) Coordination of water to magnesium cations. *Inorg. Chem.* **33**, 419–427.

Bolou-Bi B.E., Vigier N., Leyval C. and Poszwa A. (2010) Experimental determination of magnesium isotope fraction- ation during higher plant growth. *Geochim. Cosmochim. Acta* **74**, 2523–2537.

Bolou-Bi E.B., Vigier N., Poszwa A., Boudot J.-P. and Dambrine E. (2012) Effects of biogeochemical processes on magnesium isotope variations in a forested catchment in the Vosges Mountains (France). *Geochim. Cosmochim. Acta* **87**, 341–355.

Brimhall G.H. and Dietrich W.E. (1987) Constitutive mass balance relations between chemical composition, volume, density, porosity, and strain in metasomatic hydrochemical systems: results on weathering and pedogenesis. *Geochim. Cosmochim. Acta* **51**, 567–587.

Bullen T. and Chadwick O.A. (2016) Ca, Sr and Ba stable isotopes reveal the fate of soil nutrients along a tropical climosequence in Hawaii. *Chem. Geol.* **422**, 25–45.

Carrillo J.H., Hastings M.G., Sigman D.M. and Huebert B.J. (2002) Atmospheric deposition of inorganic and organic nitrogen and base cations in Hawaii. *Global Biogeochem. Cy.* **16**, 24-1–24-16.

723 Carugo O., Djinović K. and Rizzi M. (1993). Comparison of the co-ordinative behaviour of
724 calcium(II) and magnesium(II) from crystallographic data. *J. Chem. Soc. Dalton Trans.*
725 **14**, 2127–2135.
726 Chadwick O.A., Brimhall G.H. and Hendricks D.M. (1990) From a black to a gray box – a mass
727 balance interpretation of pedogenesis. *Geomorphology* **3**, 369–390.
728 Chadwick O.A., Derry L.A., Vitousek P.M., Heubert B.J. and Hedin L.O. (1999) Changing
729 sources of nutrients during four million years of ecosystem development. *Nature* **397**,
730 491–497.
731 Chadwick O.A., Gavenda R.T., Kelly E.F., Ziegler K., Olson C.G., Crawford Elliott W. and
732 Hendricks D.M. (2003) The impact of climate on the biogeochemical functioning of
733 volcanic soils. *Chem. Geol.* **202**, 195–223.
734 Chadwick O.A., Derry L.A., Bern C.R. and Vitousek P.M. (2009) Changing sources of strontium
735 to soils and ecosystems across the Hawaiian Islands. *Chem. Geol.* **267**, 64–75.
736 Chan L.-H. and Hein J.R. (2007) Lithium contents and isotopic compositions of ferromanganese
737 deposits from the global ocean. *Deep-Sea Res. II* **54**, 1147-1162.
738 Changela H.G., Bridges J.C. and Gurman S.J. (2012) Extended X-ray Absorption Fine Structure
739 (EXAFS) in Stardust tracks: constraining the origin of ferric iron-bearing minerals.
740 *Geochim. Cosmochim. Acta* **98**, 282–294.
741 Chorover J., DeChiaro M.J. and Chadwick O.A. (1999) Structural charge and cesium retention in
742 a chronosequence of tephritic soils. *Soil Sci. Soc. Am. J.* **63**, 169–177.
743 Chorover J., Amistandi M.K. and Chadwick O.A. (2004) Surface charge evolution of mineral-
744 organic complexes during pedogenesis in Hawaiian basalt. *Geochim. Cosmochim. Acta*
745 **68**, 4859–4876.
746 Crews T.E., Kitayama K., Fownes J.H., Riley R.H., Herbert D.A., Mueller-Dombois D. and
747 Vitousek P.M. (1995) Changes in soil phosphorus fractions and ecosystem dynamics
748 across a long chronesquence in Hawaii. *Ecology* **76**, 1407–1424.
749 de Villiers S. and Nelson B.K. (1999) Detection of low temperature hydrothermal fluxes by
750 seawater Mg and Ca anomalies. *Science* **285**, 721–723.
751 Derry L.A., Kurtz A.C., Ziegler K. and Chadwick O. (2005) Biological control of terrestrial
752 silica cycling and export fluxes to shtersheds. *Nature* **433**, 728–731.

753 Dessert C., Dupré B., François L.M., Schott J., Gaillardet J., Chakrapani G. and Bajpai S. (2001)
754 Erosion of Deccan Traps determined by river geochemistry: impact on the global climate
755 and the $^{87}Sr/^{86}Sr$ ratio of seawater. *Earth and Planet. Sci. Lett.* **188**, 459–474.
756 Dessert C., Dupré B., Gaillardet J., François L.M. and Allègre C.J. (2003) Basalt weathering
757 laws and the impact of basalt weathering on the global carbon cycle. *Chem. Geol.* **202**,
758 257–273.
759 Fiske R.S., Rose T.R., Swanson D.A., Champion D.E. and McGeehin J.P. (2009) Kulanaokuaiki
760 Tephra (ca. A.D. 400-1000): Newly recognized evidence for highly explosive eruptions
761 at Kilauea Volcano, Hawaii. *Geol. Soc. Am. Bull.* **121**, 712–728.
762 Galy A., Belshaw N.S., Halicz L. and O'Nions R.K. (2001) High-precision measurement of
763 magnesium isotopes by multiple-collector inductively coupled plasma mass
764 spectrometry. *Int. J. Mass Spectrom.* **208**, 89–98.
765 Galy A., Yoffe O., Janney P.E., Williams R.W., Cloquet C., Alard O., Halicz L., Wadhwa M.,
766 Hutcheon I.D., Ramon E. and Carignan J. (2003) Magnesium isotope heterogeneity of the
767 isotopic standard SRM980 and new reference materials for magnesium-isotope-ratio
768 measurements. *J. Anal. At. Spectrom.* **18**, 1352–1356.
769 Gao T., Ke S., Wang S.-J., Li F., Liu C., Lei J., Liao C. and Wu F. (2018) Constrasting Mg
770 isotopic compositions between Fe-Mn nodules and surrounding soils: Accumulation of
771 light Mg isotopes by Mg-depleted clay minerals and Fe oxides. *Geochim. Cosmochim.*
772 *Acta* **237**, 205–222.
773 Goodfellow B.W., Hilley G.E. and Chadwick O.A. (2013) Depth and character of rock
774 weathering across basalt-hosted climo- sequences on Hawaii and Kauai. *Earth Surf.*
775 *Process. Landf.* http://dx.doi.org/10.1002/esp.3505.
776 Hall P.L., Churchman G.J. and Theng B.K.G. (1985) Size distribution of allophane unit particles
777 in aqueous suspensions. *Clays Clay Miner.* **33**, 345–349.
778 Hindshaw R.S., Tosca R., Tosca N.J. and Tipper E.T. (2020) Experimental constraints on Mg
779 isotope fractionation durng clay formation: Implications for the global biogeochemical
780 cycle of Mg. *Earth and Planet. Sci. Lett.* **531**, 115980.
781 Huang F., Glessner J., Ianno A., Lundstrom C. and Zhang Z. (2009) Magnesium isotopic
782 composition of igneous rock standards measured by MC-ICP-MS. *Chem. Geol.* **268**, 15–
783 23.

784 Huang K.-J., Teng F.-Z., Wei G.-J., Ma J.-L. and Bao Z.-Y. (2012) Adsorption- and desorption-
785 controlled magnesium isotope fractionation during extreme weathering of basalt in
786 Hainan Island, China. *Earth and Planet. Sci. Lett.* **359–360**, 73–83.
787 Isupov V.P. (1999) Intercalation compounds of aluminum hydroxide. *J. Struct. Chem.* **40**, 672–
788 685.
789 Jacobson A.D. and Blum J.D. (2000) Ca/Sr and $^{87}Sr/^{86}Sr$ geochemistry of disseminated calcite in
790 Himalayan silicate rocks from Nanga Parbat: Influence on river water chemistry. *Geology*
791 **28**, 463-466.
792 Kennedy M.J., Chadwick O.A. Vitousek P.M., Derry L.A. and Hendricks D. M. (1998)
793 Changing Sources of Base Cations During Ecosystem Development, Hawaiian Islands.
794 *Geology* **26**, 1015-1018.
795 Kramer M.G., Sanderman J., Chadwick O.A., Chorover J. and Vitousek P.M. (2012) Long-term
796 carbon storage through retention of dissolved aromatic acids by reactive particles in soil.
797 *Global Change Biology* doi: 10.1111/j.1365-2486.2012.02681.x
798 Kurtz A.C., Derry L.A., Chadwick O.A. and Alfano M.J. (2000) Refractory element mobility in
799 volcanic soils. *Geology* **28**, 683–686.
800 Kurtz A.C., Derry L.A. and Chadwick O.A. (2001) Accretion of Asian dust to Hawaiian soils:
801 Isotopic, elemental, and mineral mass balances. *Geochim. Cosmochim. Acta* **65**, 1971–
802 1983.
803 Kyte F.T., Leinen M., Ross Heath G. and Zhou L. (1993) Cenozoic sedimentation history of the
804 central North Pacific: inferences from the elemental geochemistry of core LL44- GPC3.
805 *Geochim. Cosmochim. Acta* **57**, 1719–1740.
806 Ladeira A.C.Q., Ciminelli V.S.T., Duarte H.A., Alves M.C.M. and Ramos A.Y. (2001)
807 Mechanism of anion retention from EXAFS and density functional calculations: Arsenic
808 (V) adsorbed on gibbsite. *Geochim. Cosmochim. Acta* **65**, 1211–1217.
809 Laurora A., Brigatti M.F., Malferrari D., Galli E. and Rossi A. (2011) The crystal chemistry of
810 lizardite-1T from northern Apennines ophiolites near Modena, Italy. *Can. Mineral.* **49**,
811 1045–1054.
812 Lee S.-W., Ryu J.-S. and Lee K.-S. (2014) Magnesium isotope geochemistry in the Han River,
813 South Korea. *Chem. Geol.* **364**, 9–19.

814 Li W.-Y., Teng F.-Z., Ke S., Rudnick R.L., Gao S., Wu F.-Y. and Chappell B.W. (2010)
815 Heterogeneous magnesium isotopic composition of the upper continental crust. *Geochim.*
816 *Cosmochim. Acta* 74, 6867–6884.
817 Li W., Beard B.L., Li C. and Johnson C.M. (2014) Magnesium isotope fractionation between
818 brucite [$Mg(OH)_2$] and Mg aqueous species: Implications for silicate weathering and
819 biogeochemical processes. *Earth and Planet. Sci. Lett.* **394**, 82–93.
820 Ling M.-X., Sedaghatpour F., Teng F.-Z., Hays P.D., Strauss J. and Sun W. (2011) Homogenous
821 magnesium isotopic composition of seawater: an excellent geostandard for Mg isotope
822 analysis. *Rapid Commun. Mass Spectrom.* **25**, 2828–2836.
823 Liu X.-M., Teng F.-Z., Rudnick R.L., McDonough W.F. and Cummings M. (2014) Massive
824 magnesium depletion and isotopic fractionation in weathered basalts. *Geochim.*
825 *Cosmochim. Acta* **135**, 336–349.
826 MacDonald G., Abbott A.T. and Peterson F.L. (1983) *Volcanoes in the sea: The geology of*
827 *Hawaii*. University of Hawaii Press.
828 Marin-Spiotta E., Chadwick O.A., Kramer M. and Carbone M.S. (2011) Carbon delivery to deep
829 mineral horizons in Hawaiian rainforest soils. *JGR-Biogeoscience*
830 doi:10.1029/2010JG001587
831 McPhie J., Walker G.P.L. and Christiansen R.L. (1990) Phreatomagmatic and phreatic fall and
832 surge deposits from explosions at Kilauea volcano, Hawaii, 1790 A.D.: Keanakakoi Ash
833 Member. *Bull. Volcanol.* **52**, 334–354.
834 Mermut A.R. and Cano A.F. (2001) Baseline studies of the clay minerals society source clays:
835 chemical analyses of major elements. *Clays Clay Miner.* **49**, 381–386.
836 Michalski J.R., Cuadros J., Bishop J.L., Dyar M.D., Dekov V. and Fiore S. (2015) Constraints on
837 the crystal-chemistry of Fe/Mg-rich smectitic clays on Mars and links to global alteration
838 trends. *Earth Planet. Sci. Lett.* **427**, 215–225.
839 Misra S. and Froelich P.N. (2012) Lithium Isotope History of Cenozoic Seawater: Changes in
840 Silicate Weathering and Reverse Weathering. *Science* **335**, 818–823.
841 Opfergelt S., Georg R., Delvaux B., Cabidoche Y. M., Burton K. and Halliday A. (2012)
842 Mechanisms of magnesium isotope fractionation in volcanic soil weathering sequences,
843 Guade- loupe. *Earth Planet. Sci. Lett.* **341**, 176–185.

Opfergelt S., Burton K.W., Georg R.B., West A.J., Guicharnaud R.A., Sigfusson B., Siebert C., Gislason S.R. and Halliday A.N. (2014) Magnesium retention on the soil exchange complex controlling Mg isotope variations in soils, soil solutions and vegetation in volcanic soils, Iceland. *Geochim. Cosmochim. Acta* **125**, 110–130.

Pavlov M., Siegbahn P.E.M. and Sandström M. (1998) Hydration of beryllium, magnesium, calcium, and zinc ions using density functional theory. *J. Phys. Chem. A* **102**, 219–228.

Peskleway C.D., Henderson G.S. and Wick F.J. (2003) Dissolution of gibbsite: Direct observations using fluid cell atomic force microscopy. *Am. Mineral.* **88**, 18–26.

Pett-Ridge J.C., Monastra V., Derry L.A. and Chadwick O.A. (2007) Importance of atmospheric inputs and Fe-oxides in controlling soil uranium budgets and behavior along a Hawaiian chronosequence. *Chem. Geol.* **244**, 691–707.

Pogge von Strandmann P.A.E., Burton K.W., James R.H., van Calsteren P., Gislason S.R. and Sigfússon B. (2008) The influence of weathering processes on riverine magnesium isotopes in a basaltic terrain. *Earth Planet. Sci. Lett.* **276**, 187–197.

Pogge von Strandmann P.A.E., Opfergelt S., Lai Y.J., Sigfu´sson B., Gislason S.R. and Burton K.W. (2012) Lithium, magnesium and silicon isotope behaviour accompanying weathering in a basaltic soil and pore water profile in Iceland. *Earth Planet. Sci. Lett.* **339**, 11–23.

Pogge von Strandmann P.A.E., Jenkyns H.C. and Woodfine R.G. (2013). Lithium isotope evidence for enhanced weathering during Oceanic Anoxic Event 2. *Nat. Geosci.* **6**, 668–672.

Rudnick R.L. and Gao S. (2003) Composition of the continental crust. In: Rudnick RL (Ed.) *The Crust*. Treatise on Geochemistry. Elsevier-Pergamon, Oxford, pp. 1–64.

Ryu J.-S., Jacobson A.D., Holmden C., Lundstrom C. and Zhang Z. (2011) The major ion, $\delta^{44/40}$Ca, $\delta^{44/42}$Ca, and $\delta^{26/24}$Mg geochemistry of granite weathering at pH = 1 and T = 25°C: power-law processes and the relative reactivity of minerals. *Geochim. Cosmochim. Acta* **75**, 6004–6026.

Ryu J.-S., Vigier N., Lee S.-W., Lee K.-S. and Chadwick O.A. (2014) Variation of lithium isotope geochemistry during basalt weathering and secondary mineral transformations in Hawaii. *Geochim. Cosmochim. Acta* **145**, 103–115.

874 Ryu J.-S., Vigier N., Decarreau A., Lee S.-W., Lee K.-S., Song H. and Petit S. (2016)
875 Experimental investigation of Mg isotope fractionation during mineral dissolution and
876 clay formation. *Chem. Geol.* **445**, 135–145.
877 Schwertmann U. and Taylor R.M. (1989) Iron oxides. In: Dixon, J.B., and Weed, S.B., (Eds.)
878 *Minerals in Soil Environments*. 2nd ed., Soil Science Society of America Book Series 1.
879 Shannon R.D. (1976) Revised effective ionic radii and systematic studies of interatomic
880 distances in halides and chalcogenides. *Acta Cryst.* **A32**, 751-767.
881 Stewart B.W., Capo R.C., and Chadwick O.A. (2001) Effects of precipitation on weathering rate,
882 base cation provenance and Sr isotope composition in a volcanic soil climosequence,
883 Hawaii. *Geochimica et Cosmochimica Acta* **65**, 1087-1099.
884 Teng F.-Z., Li W.-Y., Rudnick R.L. and Gardner L.R. (2010) Contrasting behavior of lithium
885 and magnesium isotope fractionation during continental weathering. *Earth Planet. Sci.*
886 *Lett.* **300**, 63–71.
887 Teng F.-Z. (2017) Magnesium Isotope Geochemistry. *Rev. Mineral. Geochem.* **82**, 218–287.
888 Tipper E.T., Galy A. and Bickle M.J. (2006) Riverine evidence for a fractionated reservoir of Ca
889 and Mg on the continents: Implications for the oceanic Ca cycle. *Earth Planet. Sci. Lett.*
890 **247**, 267–279.
891 Tipper E.T., Galy A. and Bickle M.J. (2008a) Calcium and magnesium isotope systematics in
892 rivers draining the Himalaya–Tibetan-Plateau region: Lithological or fractionation
893 control? *Geochim. Cosmochim. Acta* **72**,1057–1075.
894 Tipper E.T., Louvat P., Capmas F., Galy A. and Gaillardet J. (2008b) Accuracy of stable Mg and
895 Ca isotope data obtained by MC-ICP-MS using the standard addition method. *Chem.*
896 *Geol.* **257**, 65–75.
897 Trostle K. (2014) Weathering And Magnesium Isotope Fractionation In Arid Hawaiian Soils. Ph.
898 D. thesis, Cornell Univ.
899 Vigier N., Gislason S.R., Burton K.W., Millot R. and Mokadem F. (2009) The relationship
900 between riverine lithium isotope composition and silicate weathering rates in Iceland.
901 *Earth and Planet. Sci. Lett.* **287**, 434–441.
902 Vitousek P.M., Chadwick O.A., Crew T.E., Fownes J.H., Hendricks D.M. and Herbert D. (1997)
903 Soil and Ecosystem Development Across the Hawaiian Islands. *GSA TODAY* **7**, 1–9.

Vitousek P.M. (2004) *Nutrient cycling and limitation: Hawaii as a model system*. Princeton University Press, Princeton, New Jersey, USA.

Wang W., Qin T., Zhou C., Huang S., Wu Z. and Huang F. (2017) Concentration effect on equilibrium fractionation of Mg-Ca isotopes in carbonate minerals: insights from first-principles calculations. *Geochim. Cosmochim. Acta* **208**, 185–197.

Wiegand B.A., Chadwick O.A., Vitousek P.M. and Wooden J.L. (2005) Ca cycling and isotopic fluxes in forested ecosystems in Hawaii. *Geophys. Res. Lett.* 32: L11404, doi:10.1029/2005GL022746.

Wimpenny J., Gislason S.R., James R.H., Gannoun A., Pogge von Strandmann P.A.E. and Burton K.W. (2010) The behaviour of Li and Mg isotopes during primary phase dissolution and secondary mineral formation in basalt. *Geochim. Cosmochim. Acta* **74**, 5259–5279.

Wimpenny J., Colla C.A., Yin Q.-Z., Rustad J.R. and Casey W.H. (2014) Investigating the behaviour of Mg isotopes during the formation of clay minerals. *Geochim. Cosmochim. Acta* **128**, 178–194.

Wolfe E.W. and Morris J. (1996) *Geologic Map of the Island of Hawaii*. US Geological Survey Miscellaneous Investigations Map I–2524.

Wright T.L. and Heltz R.T. (1986) Differentiation and magma mixing on Kilauea's east rift zone: a further look at the eruptions of 1955 and 1960. Part II. The 1960 lavas. *Bull. Volcanol.* **57**, 602–630.

Young E.D. and Galy A. (2004) The isotope geochemistry and cosmochemistry of magnesium. *Rev. Mineral. Geochem.* **55**, 197–230.

Zhong Y., Chen L.-H., Wang X.-J., Zhang G.-L., Xie L.-W. and Zeng G. (2017) Magnesium isotopic variation of oceanic island basalts generated by partial melting and crustal recycling. *Earth and Planet. Sci. Lett.* **463**, 127–135.

Ziegler K., Chadwick O.A., Brzezinski M.A. and Kelly E.F. (2005) Natural variations of $\delta^{30}Si$ ratios during progressive basalt weathering, Hawaiian Islands. *Geochim. Cosmochim. Acta* **69**, 4597–4610.

Zieman J.J., Holmes J.L., Connor D., Jensen C.R. and Zoller W.H. (1995) Atmospheric erosol trace element chemistry at Mauna Loa Observatory. *J. Geophys. Res.* **100**, 25979–25994.

FIGURE CAPTIONS

Figure 1. Elemental concentrations and the elemental gain ($\tau_{j,w} > 0$) or loss ($\tau_{j,w} < 0$) versus depth. (a)-(c) Concentrations of Mg, Al and Fe in each soil profile. (d)-(f) τ_{Mg} is calculated using Eq. (1). All [Mg], [Al], [Fe] and [Nb] data in parent basalts are from Ziegler et al. (2005). (see text for more details).

Figure 2. Magnesium isotope compositions versus depth. The black and blue lines represent average δ^{26}Mg values of –0.26‰ (Hawaiian basalts; Zhong et al., 2017) and –0.83‰ (seawater; Ling et al., 2011), respectively.

Figure 3. Depth-integrated parameters versus age. (a) The Mg gain or loss (τ_{Mg}), (b) δ^{26}Mg, (c)-(f) Mineralogical compositions (Ziegler et al., 2005). The black line in (b) represents average δ^{26}Mg value of –0.26‰ in Hawaiian basalts (Zhong et al., 2017). Error bars are smaller than the symbols.

Figure 4. Magnesium isotopic compositions in the labile and residual Mg as a function of age. (a) Organic-rich surface soils and (b) Subsurface soils. The colored-lines represent seawater (blue; –0.83‰; Ling et al., 2011), basalt (black; –0.26‰; Zhong et al., 2017), plant (green; –0.07‰; Trostle, 2014) and SOM (brown; +0.06‰; Trostle, 2014), respectively.

Figure 5. δ^{26}Mg values versus 1/[Mg] (wt.%$^{-1}$) for the labile and residual Mg in all soil samples measured in this study. Asian dust δ^{26}Mg is assumed to be equal to the upper continental crust (UCC) δ^{26}Mg (–0.22‰; Li et al., 2010) with [Mg] of 1.5 wt.% (Rudnick and Gao, 2014). Plant δ^{26}Mg is –0.07±0.26‰ (2σ, n=4; Trostle, 2014) with [Mg] of 0.15±0.12 wt.% (2σ, n=4; Trostle, 2014), SOM δ^{26}Mg is +0.06±0.48‰ (2σ, n=4; Trostle, 2014)

with [Mg] of 0.03±0.02 wt.% (2σ, n=4; Trostle, 2014), rainwater δ^{26}Mg is assumed to be equal to seawater δ^{26}Mg (–0.83‰; Ling et al., 2011) with [Mg] of 0.09±0.11 ppm (2σ, n=6; Carrillo et al., 2002), and Hawaiian basalts δ^{26}Mg is –0.26±0.06‰ (2σ, n=11; Zhong et al., 2017) with [Mg] of 4.7±1.6 wt.% (2σ, n=10; Zhong et al., 2017). The grey shaded field marks the mixing zone between each considered end-member. Error bars for soil samples are smaller than the symbols. Data for a cross symbol are from Opfergelt et al. (2014). Symbols are the same as in Fig. 2.

Figure S1. Map of the Hawaiian Islands showing the sampling locations and their substrate ages (Modified from Crews et al., 1995).

Figure S2. Fraction of each end-member (basalt, dust and rainwater) relative to the total Mg (%) versus age. Error bars represent 1σ, propagated using the range of [Mg] for each end-member (see text for more details).

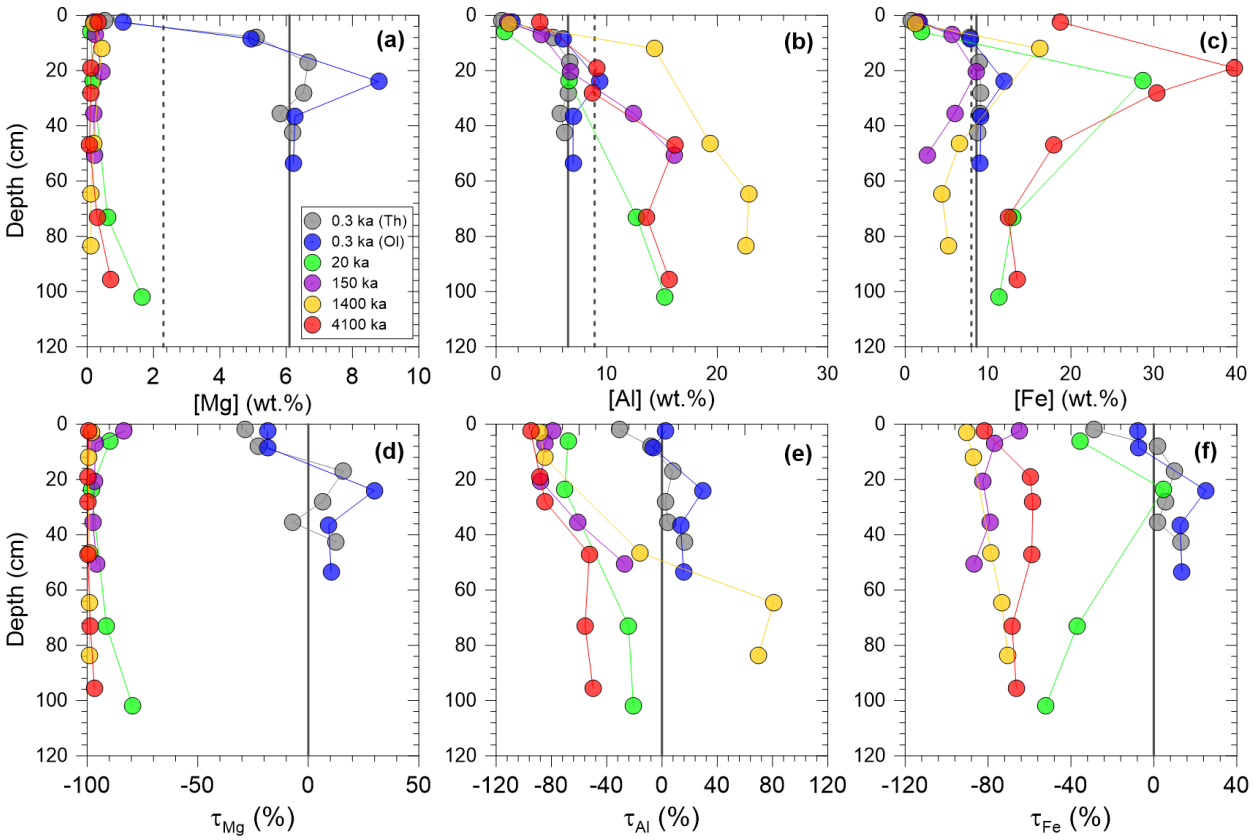

Fig. 1. Ryu *et al.*

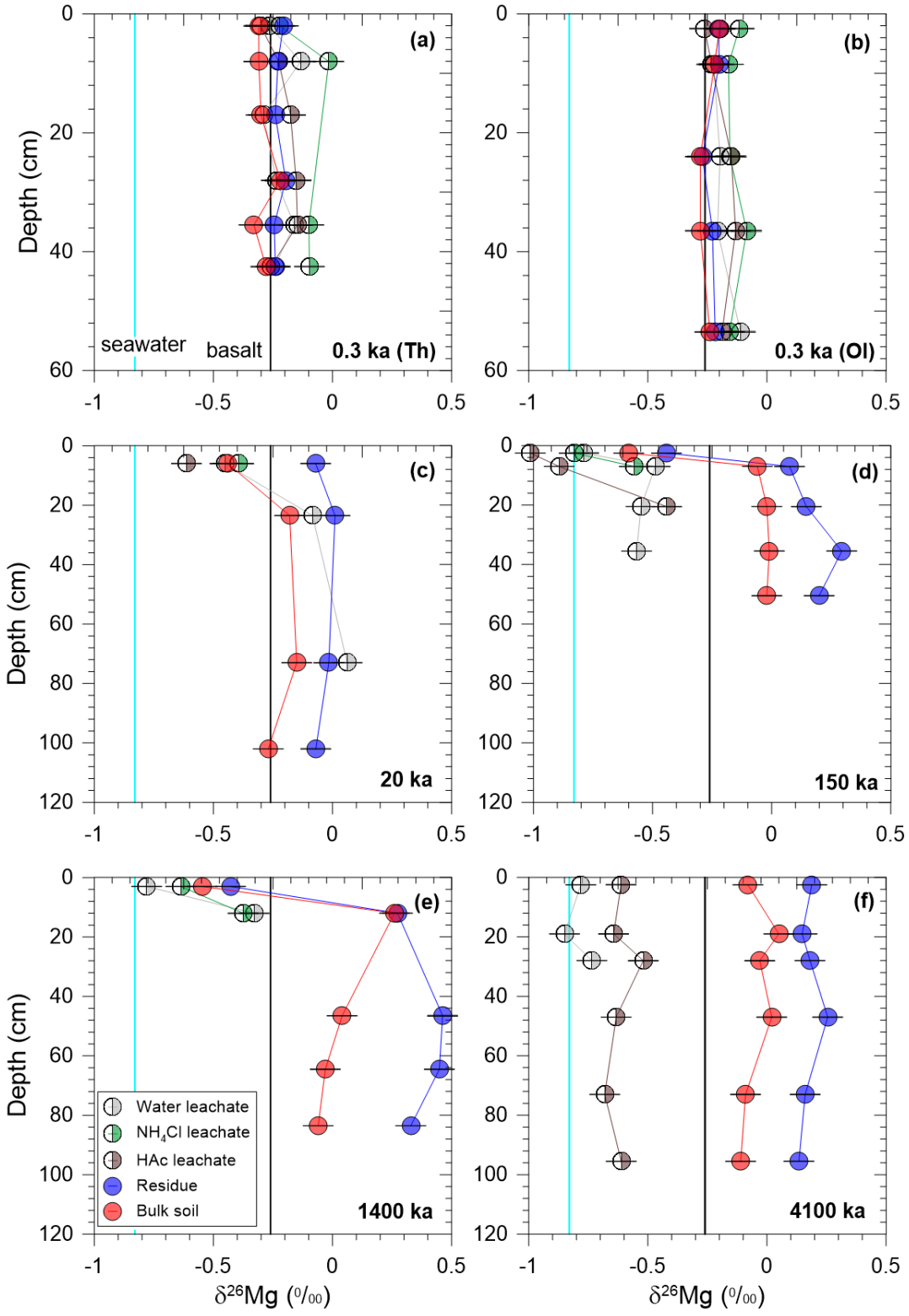

Fig. 2. Ryu *et al.*

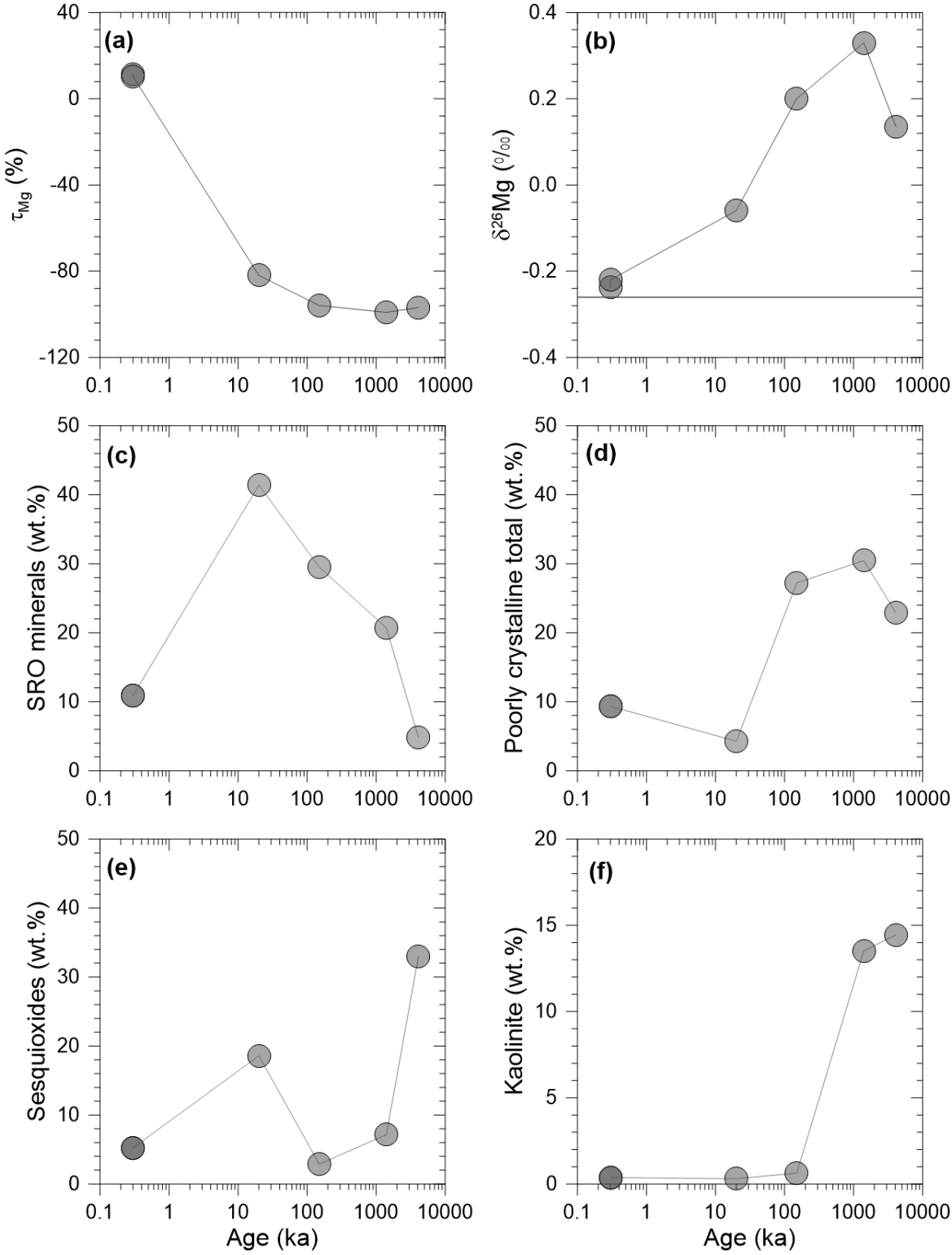

Fig. 3. Ryu *et al.*

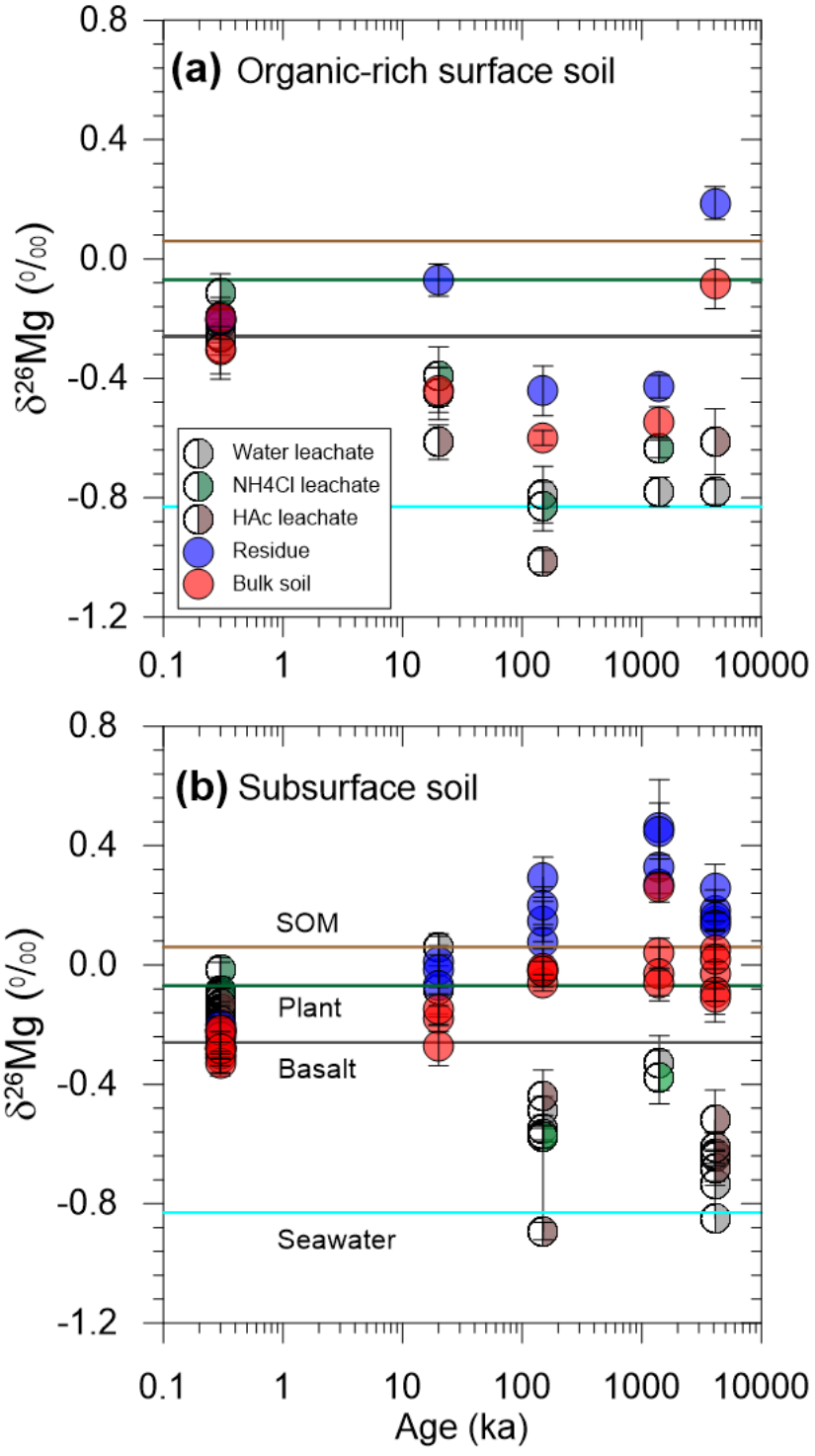

Fig. 4. Ryu *et al.*

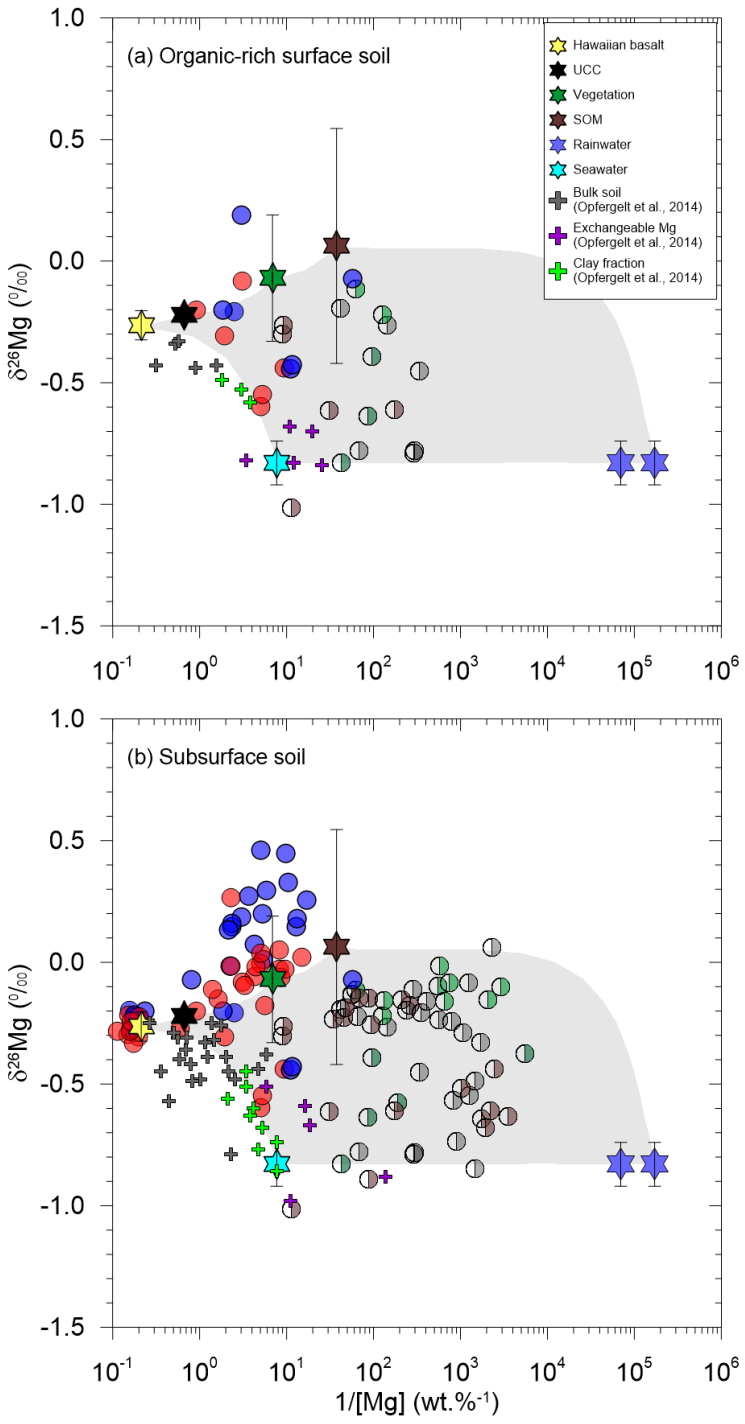

Fig. 5. Ryu *et al.*

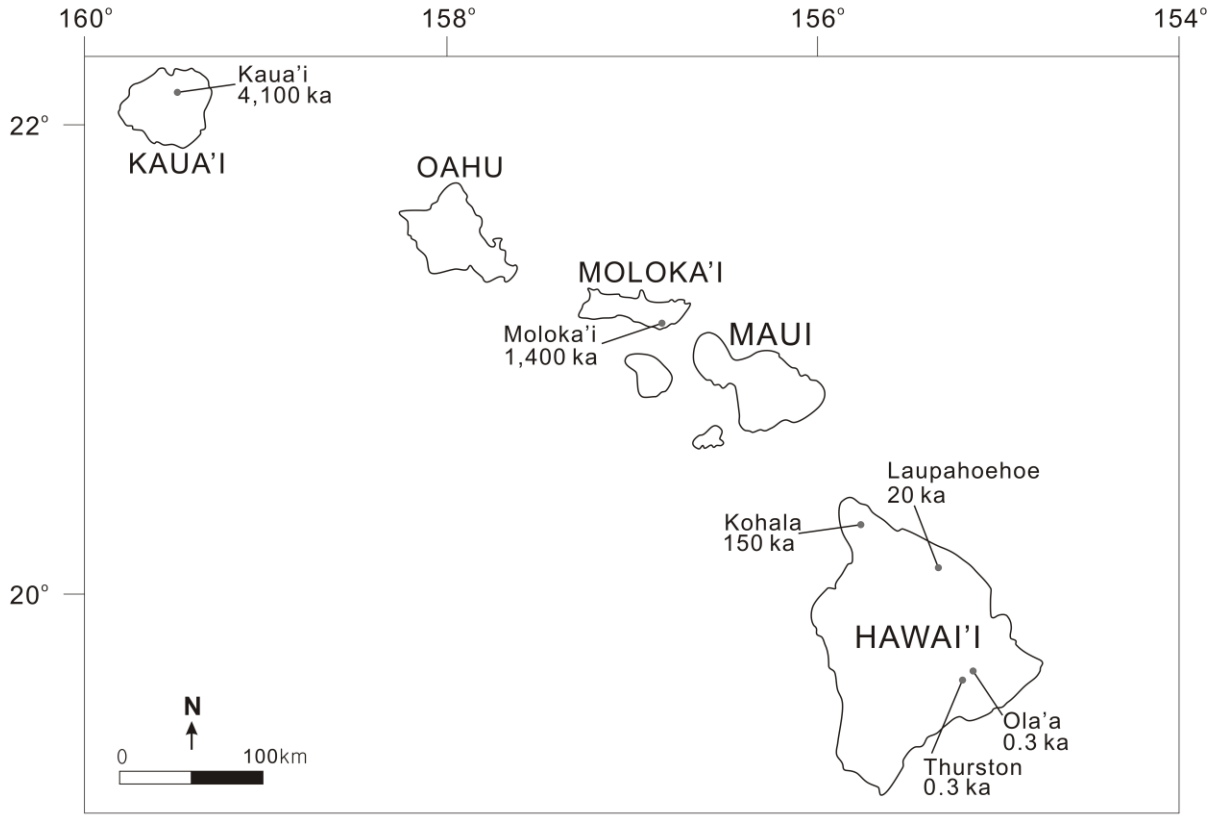

Fig. S1. Ryu *et al.*

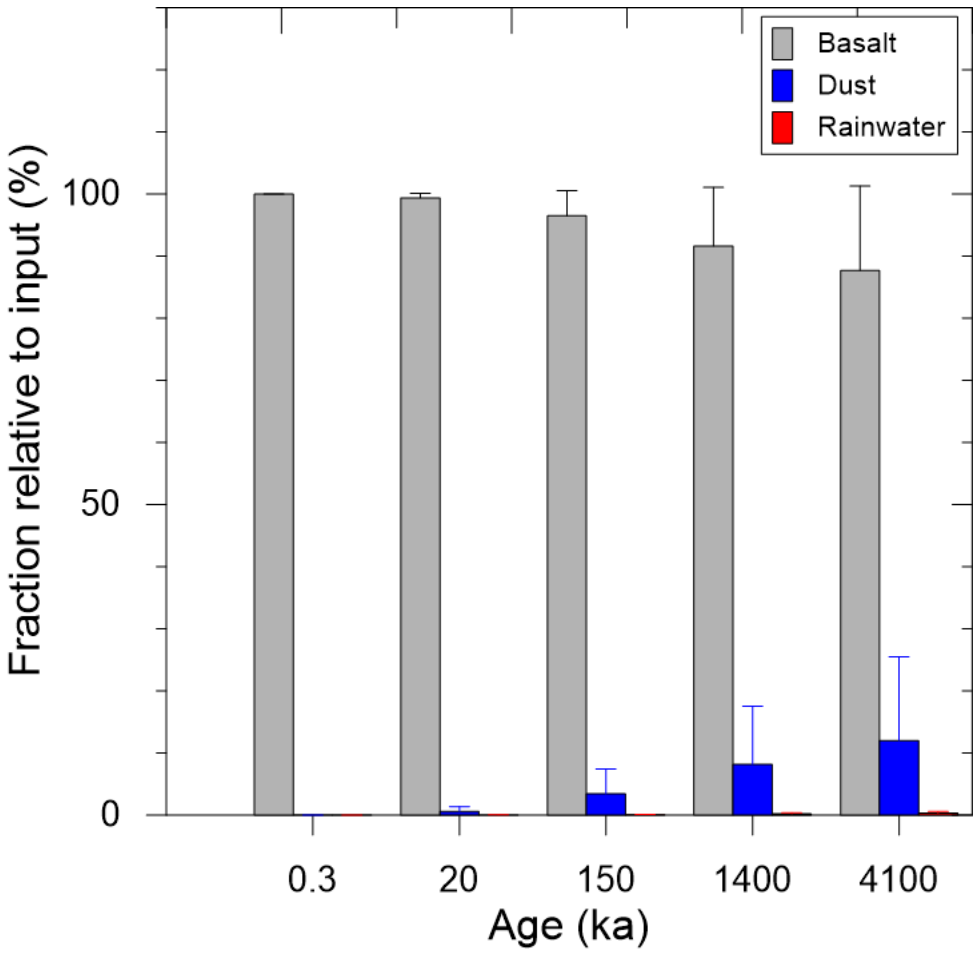

Fig. S2. Ryu *et al.*